Eidgenössische Technische Hochschule Zürich

Ecole polytechnique fédérale de Zurich
Politecnico federale di Zurigo
Swiss Federal Institute of Technology Zurich

Convergence analysis with parameter estimates for a reduced basis acoustic scattering T-matrix method

M. Ganesh*, S.C. Hawkins† and R. Hiptmair

Research Report No. 2011-04
February 2011

Seminar für Angewandte Mathematik
Eidgenössische Technische Hochschule
CH-8092 Zürich
Switzerland

*Department of Mathematical and Computer Sciences, Colorado School of Mines, Golden, USA

†Department of Mathematics, Macquarie University, Sydney, Australia

Convergence analysis with parameter estimates for a reduced basis acoustic scattering T-matrix method

M. Ganesh* S. C. Hawkins† R. Hiptmair‡

Abstract

The reduced basis method is an offline/online process for the approximation of functional outputs of parameterized mathematical models. The offline process is for solutions of the models for a reduced finite set of parameters and the online process provides the option of quickly obtaining the functional outputs for an infinite choice of parameters in the model. For reliability of the offline/online process, it is important to establish convergence analysis of the reduced basis method and provide a practical estimate for optimal reduction of parameters. The choice of reduced parameters is usually obtained using some optimization technique.

For wave propagation models, with the parameters being incident waves and directions, the celebrated T-matrix method is an optimization-free reduced basis method. However, establishing convergence analysis and providing practical estimates of truncation parameters for the T-matrix method has remained an open problem for several decades. In this work we solve this open problem, for time-harmonic acoustic scattering in two and three dimensions, with an optimization-free reduced basis T-matrix method. We numerically demonstrate the convergence analysis and parameter estimates for both point-source and plane-wave incident waves. Our approach can be used in conjunction with any numerical method for solving the forward wave propagation problem.

Key words: Wave propagation, Acoustic Scattering, T-matrix

AMS subject classifications: 65R20, 65N35.

Running title: T-matrix convergence analysis

*Department of Mathematical and Computer Sciences, Colorado School of Mines, Golden, CO 80401. (mganesh@mines.edu)

†Department of Mathematics, Macquarie University, Sydney, NSW 2109, Australia. (stuart.hawkins@mq.edu.au)

‡Seminar für Angewandte Mathematik, ETH Zurich, CH-8092 Zürich. (hiptmair@sam.math.ethz.ch)

1 Introduction

The fast simulation of wave propagation induced by *various* types of incident waves, impinging on a fixed bounded three dimensional configuration (scatterer) from *several* directions, is fundamental to several applications. In modern applications, the type of incident wave and associated incident directions are chosen by the end user, who requires certain online information quickly, while the shape of the configuration remains fixed (or based on a few prototype shapes). That is, the end users are given infinite parameter options. The online requirements are typically functional outputs (such as the intensity or radar cross section) of mathematical models describing the wave propagation.

In such cases, independent of the user input, it is efficient to *a priori* construct and store certain tools that completely characterize (up to certain accuracy) the essential scattering properties of the prototype configurations (using offline computations of appropriately discretized mathematical models) so that online information can be simulated very quickly by end users, for example using simple matrix-vector multiplications, for *any* parameter choice. Here, the matrix describes the essential properties of the configuration and the vector is the input chosen by the end user.

In general, full mathematical models of physical processes contain some user input parameters. A framework that provides the end user with infinite (online) choice of input parameters by first solving (offline) the full model for only a reduced class of finite number parameters is known as the reduced basis method, see [2, 16] and extensive references therein for various applications. For a chosen application/model, fundamental questions in the reduced basis method are: (i) which choice of basis sets should be used to represent the functional outputs of the full models and the input functions (so that the output and input functions can be represented by vectors); (ii) how to provide a robust and practical *a priori* (or *a posteriori*) estimate of the cardinality of the reduced basis sets; and (iii) how to establish a full convergence analysis of the associated reduced basis method.

In this work we propose a class of spectral reduced basis method for time-harmonic acoustic scattering in two and three dimensions, with user input parameters being the practically important types of incident wave:

(i) a plane wave with arbitrary incident direction;

(ii) the field generated by a point-source with arbitrary location.

The standard reduced basis methods for most applications require some form of expensive optimization procedures to choose the reduced set of parameters. However, for the application considered in this work, the optimization cost can be completely avoided.

The T-matrix method is an optimization-free reduced basis method for our application. The T-matrix was first introduced for wave propagation over half a century ago in [17] and the standard truncated T-matrix method has been widely used since then, see [5, 13, 14, 15] and extensive references therein. The basis sets for the standard T-matrix method consist of the classical wave functions.

It is well known that the standard T-matrix method, which uses the null field method, is numerically unstable and for large obstacles can become divergent [15, p. 543]. There are several approaches to tackle this problem [5, 13, 14, 15], such as using slow extended

precision arithmetic to minimize the effect of round-off errors. The numerical instability arises mainly due to the use of near-fields to compute entries of the reduced basis T-matrix and fast growth of Hankel functions in the basis sets. In a recent work for acoustic scattering [13, §7.9.4] it was suggested that the instability could be avoided by using far fields, and the instability was computationally avoided in a robust way in [9, 10] using far fields of the Hankel functions.

The standard T-matrix method has been investigated in the literature mainly for plane-wave incidence, with the end user supplied parameter being the arbitrary incident direction. Despite being widely used over the last five decades, it has been an open-problem to establish a robust convergence analysis of any T-matrix method and to provide a precise *a priori* parameter estimates to efficiently truncate the T-matrix, even for plane-wave incidence. While there have been several advances in the convergence analysis and parameter estimates for several optimization-based reduced basis methods [2, 16], the lack of convergence analysis and parameter estimates for the optimization-free reduced basis T-matrix method has been considered a major disadvantage.

The main aim of this work is to avoid this major disadvantage by answering all three fundamental questions, for an optimization-free reduced basis method with practically important point-source and plane-wave incidence with their source locations or wave directions as free user input parameters. In addition to providing *a priori* estimates for the truncation parameters and proving exponential convergence of the reduced basis T-matrix method, we demonstrate the theory and estimates using several numerical experiments for two and three dimensional acoustic scattering.

2 Acoustic obstacle scattering

We consider the model problem of time-harmonic exterior acoustic obstacle scattering in $\mathbb{R}^d$ for $d = 2, 3$. Let $D \subset \mathbb{R}^d$ be a bounded sound-soft or sound-hard or absorbing scatterer in a homogeneous medium. The coordinate system is chosen so that the origin $\mathbf{0}$ is inside D. Let $\rho_D > 0$ be the radius of the scatterer with respect to the origin, so that $D \subset B_{\rho_D}$, where $B_{\rho_D} \subset \mathbb{R}^d$ denotes the ball with center $\mathbf{0}$ and radius ρ_D.

Let $u^{\rm inc}$ be an incident wave with wavelength $\lambda = 2\pi/k$, where k is the wavenumber, impinging on the scatterer D. The resulting time-harmonic radiating acoustic scattered field $u^{\rm s}$ scattered by D satisfies the Helmholtz equation [4, Sect. 2.1],

$$\triangle u(\boldsymbol{x}) + k^2 u(\boldsymbol{x}) = 0\,, \quad \boldsymbol{x} \in \mathbb{R}^d \setminus \overline{D}\,, \tag{2.1}$$

and one of the following boundary conditions (*properties of the scatterer*)

$$u^{\rm s}(\boldsymbol{x}) = -u^{\rm inc}(\boldsymbol{x})\,, \qquad \text{(sound-soft)} \tag{2.2}$$

$$\frac{\partial u^{\rm s}}{\partial \boldsymbol{n}}(\boldsymbol{x}) = -\frac{\partial u^{\rm inc}}{\partial \boldsymbol{n}}(\boldsymbol{x})\,, \qquad \text{(sound-hard)} \tag{2.3}$$

$$u^{\rm s}(\boldsymbol{x}) + \lambda \frac{\partial u^{\rm s}}{\partial \boldsymbol{n}}(\boldsymbol{x}) = -u^{\rm inc}(\boldsymbol{x}) - \lambda \frac{\partial u^{\rm inc}}{d\boldsymbol{n}}(\boldsymbol{x})\,, \quad \mathrm{Im}(\lambda) > 0, \qquad \text{(absorbing)} \tag{2.4}$$

for $\boldsymbol{x} \in \partial D$, and the Sommerfeld radiation condition

$$\lim_{|\boldsymbol{x}| \to \infty} |\boldsymbol{x}|^{(d-1)/2} \left(\frac{\partial u}{\partial |\boldsymbol{x}|} - iku \right) = 0, \tag{2.5}$$

where the limit holds uniformly in all directions $\widehat{\boldsymbol{x}} = \boldsymbol{x}/|\boldsymbol{x}| \in \mathbb{S}^{d-1}$, and $\mathbb{S}^{d-1}$ is the unit sphere in $\mathbb{R}^d$ for $d = 2, 3$. Furthermore, the radiating solution $u^{\rm s}$ has the asymptotic behaviour of an outgoing spherical wave [4, Theorem 2.5]:

$$u^{\rm s}(\boldsymbol{x}) = \frac{e^{ik|\boldsymbol{x}|}}{|\boldsymbol{x}|^{(d-1)/2}} \left\{ u^\infty(\widehat{\boldsymbol{x}}) + O\left(\frac{1}{|\boldsymbol{x}|}\right) \right\}, \tag{2.6}$$

as $|\boldsymbol{x}| \to \infty$ uniformly in all directions $\widehat{\boldsymbol{x}} = \boldsymbol{x}/|\boldsymbol{x}|$. The function u^∞ defined on $\mathbb{S}^{d-1}$ in (2.6) is known as the *far field pattern* of u. Thus the far field $u^\infty \in L^2(\mathbb{S}^{d-1})$ has the representation

$$u^\infty(\widehat{\boldsymbol{x}}) = \lim_{|\boldsymbol{x}|\to\infty} |\boldsymbol{x}|^{(d-1)/2} e^{-ik|\boldsymbol{x}|} u^{\rm s}(\boldsymbol{x}), \qquad \widehat{\boldsymbol{x}} = \boldsymbol{x}/|\boldsymbol{x}|. \tag{2.7}$$

Computation of the far field pattern plays an important role in inverse scattering to identify the shape of the scatterer [4, Ch. 5].

For expanding the incident, scattered, and far fields using a new class of elementary regular and radiating functions, and to unify notation in two and three dimensions, we introduce the infinite index sets

$$\mathbb{I}_d = \begin{cases} \{\boldsymbol{\ell} = \ell : \ell \in \mathbb{Z}\}, & \text{for } d = 2, \\ \\ \{\boldsymbol{\ell} = (\ell, j) : \ell \in \mathbb{N}_0, |j| \le \ell\}, & \text{for } d = 3, \end{cases}$$

and finite subsets

$$\mathbb{I}_{d,N} = \begin{cases} \{\boldsymbol{\ell} = \ell : -N \le |\ell| \le N\}, & \text{for } d = 2, \\ \\ \{\boldsymbol{\ell} = (\ell, j) : 0 \le \ell \le N, |j| \le \ell\}, & \text{for } d = 3, \end{cases}$$

where $\mathbb{N}_0 = \mathbb{N} \cup \{0\}$. For $\boldsymbol{\ell} \in \mathbb{I}_d$, with $\boldsymbol{\ell} = \ell$ or $\boldsymbol{\ell} = (\ell, j)$, we use the notation $|\boldsymbol{\ell}| = |\ell|$.

Let N_d denote the cardinality of $\mathbb{I}_{d,N}$. We have

$$N_d = \begin{cases} 2N + 1 & d = 2, \\ \\ (N+1)^2, & d = 3. \end{cases} \tag{2.8}$$

Throughout the paper, for $\boldsymbol{\ell} \in \mathbb{I}_d$, the functions $J_{|\boldsymbol{\ell}|}$, $j_{|\boldsymbol{\ell}|}$, $H^{(1)}_{|\boldsymbol{\ell}|}$, and $h^{(1)}_{|\boldsymbol{\ell}|}$ are respectively the Bessel, spherical-Bessel, Hankel, and spherical-Hankel functions of degree $|\boldsymbol{\ell}|$. For $\boldsymbol{\ell} = (\ell, j) \in \mathbb{I}_3$, we denote by $Y_{l,j}$ the spherical harmonic of degree l, given by

$$Y_{\ell,j}(\widehat{\boldsymbol{x}}) = (-1)^{(j+|j|)/2} \sqrt{\frac{2l+1}{4\pi} \frac{(l-|j|)!}{(l+|j|)!}} P_\ell^{|j|}(\cos\theta) e^{ij\phi}, \qquad \widehat{\boldsymbol{x}} \in \mathbb{S}^2, \tag{2.9}$$

where $P_\ell^{|j|}$ is the associated Legendre function of degree ℓ and index j. Here we have used the spherical polar coordinates representation of the unit vector $\widehat{\boldsymbol{x}}$ with polar angle θ and azimuth ϕ. Formally, for $\boldsymbol{x} \in \mathbb{R}^2$ we write

$$\boldsymbol{x} = \boldsymbol{x}(\theta) = |\boldsymbol{x}|\widehat{\boldsymbol{x}} = |\boldsymbol{x}|(\cos\theta, \sin\theta)^T$$

and for $\boldsymbol{x} \in \mathbb{R}^3$ we write

$$\boldsymbol{x} = \boldsymbol{x}(\theta, \phi) = |\boldsymbol{x}|\widehat{\boldsymbol{x}} = |\boldsymbol{x}|(\sin\theta\cos\phi, \sin\theta\sin\phi, \cos\theta)^T.$$

We consider the orthonormal basis functions in $L^2(\mathbb{S}^{d-1})$ given by

$$Y_{\boldsymbol{\ell}}(\widehat{\boldsymbol{x}}) = \begin{cases} \frac{1}{\sqrt{2\pi}}\exp(i\ell\theta), & d = 2, \\ \\ Y_{\ell,j}(\widehat{\boldsymbol{x}}), & d = 3, \end{cases} \qquad \widehat{\boldsymbol{x}} \in \mathbb{S}^{d-1},\ \ell \in \mathbb{I}_d. \tag{2.10}$$

In applications, the incident field u^{inc} is frequently an incident *plane wave* with propagation direction $\widehat{\boldsymbol{d}} \in \mathbb{S}^{d-1}$, and the far field pattern u^∞ is the functional output of interest. In particular, one might like to know the acoustic cross section (ACS) of the scatterer at *any* user chosen direction $\widehat{\boldsymbol{x}} \in \mathbb{S}^{d-1}$, defined by

$$\sigma(\widehat{\boldsymbol{x}}; \widehat{\boldsymbol{d}}) = 4\pi|u^\infty(\widehat{\boldsymbol{x}})|^2. \tag{2.11}$$

A derived quantity of interest is the monostatic ACS, which is computed with $\widehat{\boldsymbol{d}} = -\widehat{\boldsymbol{x}}$. For the monostatic ACS , especially for non-convex configurations, the full wave propagation model needs to be solved for thousands of incident directions $\widehat{\boldsymbol{d}}$ (representing the ACS from all directions). This requires a fast implementation of the far field mapping $\widehat{\boldsymbol{d}} \mapsto u^\infty$. Another practically important class of incident waves are the circular and spherical waves generated by a point-source (located outside but possibly close to the configuration).

In this work, using a new class of basis functions, we first design an efficient offline computation to construct a matrix that is *independent* of the user input u^{inc} and that characterizes scattering properties of the configuration pair $(\partial D, k)$ so that, given a user input u^{inc}, an approximate functional-output, the ACS, can be quickly computed online using cheap matrix-vector multiplication.

2.1 Basis functions for expansion of fields

The unknown quantity in the ACS formula (2.11) is the far-field u^∞. Using (2.6) and the orthonormal basis in (2.10), since the far field $u^\infty \in L^2(\mathbb{S}^{d-1})$, there exists a sequence $\boldsymbol{a} = (a_{\boldsymbol{\ell}'})_{\boldsymbol{\ell}' \in \mathbb{I}_d}$ such that

$$u^\infty(\widehat{\boldsymbol{x}}) = \sum_{\boldsymbol{\ell}' \in \mathbb{I}_d} a_{\boldsymbol{\ell}'} Y_{\boldsymbol{\ell}'}(\widehat{\boldsymbol{x}}), \qquad \widehat{\boldsymbol{x}} \in \mathbb{S}^{d-1}. \tag{2.12}$$

An approximate far field pattern can be obtained by truncating the expansion (2.12) to N_d' terms, that is, reducing the basis to N_d' functions. *A priori* error bounds may guide the choice of N_d' and to establish them is the goal of this paper.

Hereafter let $R > \rho_D$ be a fixed positive number to be read as the radius of a ball strictly containing D, see Figure 1 (and Figures 11–12). The incident field u^{inc} solves the Helmholtz equation (2.1) everywhere inside B_R.

To motivate our approach, we first consider the incident field u^{inc} induced by a point-source located at $\boldsymbol{x}_0 \in \mathbb{R}^3$, with $|\boldsymbol{x}_0| > R$. Using [4, Theorem 2.10], we have the series representation

$$u^{\text{inc}}(\boldsymbol{x}) = \frac{\exp(ik|\boldsymbol{x} - \boldsymbol{x}_0|)}{k|\boldsymbol{x} - \boldsymbol{x}_0|} = \sum_{\boldsymbol{\ell} \in \mathbb{I}_d} p_{\boldsymbol{\ell}}\ j_{|\boldsymbol{\ell}|}(k|\boldsymbol{x}|)\ Y_{\boldsymbol{\ell}}(\widehat{\boldsymbol{x}}), \tag{2.13}$$

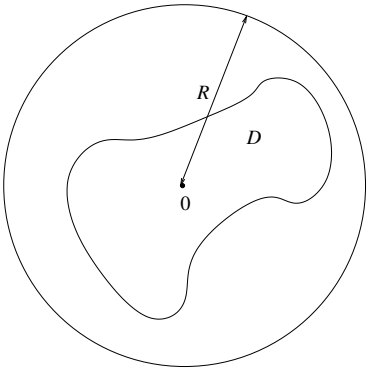

Figure 1: Geometric arrangement for the acoustic scattering problem ($d = 2$).

with expansion coefficients

$$p_{\boldsymbol{\ell}} = 4\pi i k \; h^{(1)}_{|\boldsymbol{\ell}|}(k|\boldsymbol{x}_0|) \; \overline{Y_{\boldsymbol{\ell}}(\widehat{\boldsymbol{x}}_0)}. \tag{2.14}$$

A similar expansion holds for any point-source radiation in two dimensions, using Graf's addition theorem [1, 9.1.79]. Also, truncation to N_d terms, that is, those terms satisfying $|\ell| \leq N$, may be employed in (2.13).

In this article we provide a precise *a priori* bound for the error caused by the simultaneous truncation of (2.12) and (2.13). We establish exponential convergence of the resulting approximation error as both N' and N tend to ∞. Throughout the paper C stands for a generic positive constant, whose value may differ between different occurrences. The constant may depend only on the shape of D, the boundary conditions, the separation distance R, and the wavenumber k. The constant does not depend on the truncation indices N and N' nor on the excitation u^{inc}.

After fixing N' and N, the offline task in this work is to compute an $N'_d \times N_d$ matrix so that the unknown reduced N'_d coefficients $a_{\boldsymbol{\ell}'}$ of the far-field in (2.12) can be computed online using *any* N_d input incident field coefficients $p_{\boldsymbol{\ell}}$ via a cheap matrix vector product.

Motivated by (2.13), we introduce a new class of scaled elementary wave functions:

$$\widetilde{E}_{\boldsymbol{\ell}}(\boldsymbol{x}) = \begin{cases} H^{(1)}_{|\boldsymbol{\ell}|}(kR) J_{|\boldsymbol{\ell}|}(k|\boldsymbol{x}|) Y_{\boldsymbol{\ell}}(\widehat{\boldsymbol{x}}), & d = 2, \\ \\ h^{(1)}_{|\boldsymbol{\ell}|}(kR) j_{|\boldsymbol{\ell}|}(k|\boldsymbol{x}|) Y_{\boldsymbol{\ell}}(\widehat{\boldsymbol{x}}), & d = 3, \end{cases} \qquad \boldsymbol{\ell} \in \mathbb{I}_d. \tag{2.15}$$

The scaled wave functions are unbounded entire solutions of the Helmholtz equation (2.1) and can be regarded as "incident circular/spherical waves". The scaling factors applied to the usual regular wave functions are introduced in (2.15) to ensure boundedness of coefficients in the incident field expansion for incident point source waves. The waves (2.15) decay exponentially towards the origin.

Lemma 2.1 *With constants C depending only on D and kR,*

$$\left\| \widetilde{E}_{\boldsymbol{\ell}} \restriction \partial D \right\|_{L^2(\partial D)} \leq C \left(\frac{\rho_D}{R} \right)^{|\boldsymbol{\ell}|}, \quad \forall \boldsymbol{\ell} \in \mathbb{I}_d \, , \tag{2.16}$$

$$\left\| \nabla \widetilde{E}_{\boldsymbol{\ell}} \restriction \partial D \right\|_{L^2(\partial D)} \leq C \left(\frac{\rho_D}{R} \right)^{|\boldsymbol{\ell}|-1} |\boldsymbol{\ell}|^{d/2-1}, \quad \forall \boldsymbol{\ell} \in \mathbb{I}_d, \; |\boldsymbol{\ell}| > 0 \, . \tag{2.17}$$

Proof. We make use of the fact [4, Sect. 2.4, 3.4] that, with $C > 0$ depending on kR ,

$$\max\left\{|H^{(1)}_{|\boldsymbol{\ell}|}(kR)J_{|\boldsymbol{\ell}|+\sigma}(kR)|, |h^{(1)}_{|\boldsymbol{\ell}|}(kR)j_{|\boldsymbol{\ell}|+\sigma}(kR)|\right\} \leq C|\boldsymbol{\ell}|^{\sigma-1} \quad \forall \boldsymbol{\ell} \in \mathbb{I}_d\,, \quad \begin{array}{l}\sigma \in \{-1,0,1\}\,,\\ \sigma + |\boldsymbol{\ell}| \geq 0\,,\end{array} \tag{2.18}$$

and of the estimate (see [4, Page 31] for $d = 3$, and [4, (3.57), (3.58)] for $d = 2$)

$$\left|\frac{J_{|\boldsymbol{\ell}|}(k|\boldsymbol{x}|)}{J_{|\boldsymbol{\ell}|}(kR)}\right|, \left|\frac{j_{|\boldsymbol{\ell}|}(k|\boldsymbol{x}|)}{j_{|\boldsymbol{\ell}|}(kR)}\right| \leq C\left(\frac{|\boldsymbol{x}|}{R}\right)^{|\boldsymbol{\ell}|} \quad \forall \boldsymbol{\ell} \in \mathbb{I}_d,\ |\boldsymbol{x}| \leq R\,. \tag{2.19}$$

We combine this with (2.18) and the bound (see [6, Lemma 3.1.5] for $d = 3$)

$$|Y_{\boldsymbol{\ell}}(\widehat{\boldsymbol{x}})| \leq C|\boldsymbol{\ell}|^{d/2-1}, \quad \widehat{\boldsymbol{x}} \in \mathbb{S}^{d-1}, \tag{2.20}$$

in (2.15) to obtain

$$|\widetilde{E}_{\boldsymbol{\ell}}(\boldsymbol{x})| \leq C\left(\frac{|\boldsymbol{x}|}{R}\right)^{|\boldsymbol{\ell}|} \quad \forall \boldsymbol{\ell} \in \mathbb{I}_d,\ |\boldsymbol{x}| < R\,, \tag{2.21}$$

which immediately yields the estimate for $\left\|\widetilde{E}_{\boldsymbol{\ell}}\restriction\partial D\right\|_{L^2(\partial D)}$ in (2.16).

The proof of the second estimate starts from

$$\left\|\nabla\widetilde{E}_{\boldsymbol{\ell}}\restriction\partial D\right\|_{L^2(\partial D)} \leq |\partial D|^{1/2}\left\|\nabla\widetilde{E}_{\boldsymbol{\ell}}\restriction\partial D\right\|_{L^\infty(\partial D)}\,, \tag{2.22}$$

where $|\partial D|$ denotes the surface area of ∂D, and the polar/spherical coordinate representation for $|\boldsymbol{\ell}| > 0$

$$\nabla\widetilde{E}_{\boldsymbol{\ell}}(\boldsymbol{x}) = \begin{cases} H^{(1)}_{|\boldsymbol{\ell}|}(kR)\big(kJ'_{|\boldsymbol{\ell}|}(k|\boldsymbol{x}|)Y_{\boldsymbol{\ell}}(\widehat{\boldsymbol{x}})\widehat{\boldsymbol{x}} + \frac{1}{|\boldsymbol{x}|}J_{|\boldsymbol{\ell}|}(k|\boldsymbol{x}|)\nabla^*Y_{\boldsymbol{\ell}}(\widehat{\boldsymbol{x}})\big), & d = 2\,,\\ h^{(1)}_{|\boldsymbol{\ell}|}\big(kR\big)(kj'_{|\boldsymbol{\ell}|}(k|\boldsymbol{x}|)Y_{\boldsymbol{\ell}}(\widehat{\boldsymbol{x}})\widehat{\boldsymbol{x}} + \frac{1}{|\boldsymbol{x}|}j_{|\boldsymbol{\ell}|}(k|\boldsymbol{x}|)\nabla^*Y_{\boldsymbol{\ell}}(\widehat{\boldsymbol{x}})\big), & d = 3\,,\end{cases} \tag{2.23}$$

where ∇^* is the $\mathbb{S}^{d-1}$ surface gradient. For $|\boldsymbol{\ell}| > 0$, using the formulas [1]

$$2J'_{|\boldsymbol{\ell}|} = J_{|\boldsymbol{\ell}|-1} - J_{|\boldsymbol{\ell}|+1} \quad , \quad j_{|\boldsymbol{\ell}|}(t) = \sqrt{\frac{\pi}{2t}}J_{|\boldsymbol{\ell}|+1/2}(t),\ t \geq 0\,, \tag{2.24}$$

we get the surface gradient bound (see [6, Lemma 12.6.7] for $d = 3$ and note the scaling term in [6, Equation (12.2.1)])

$$|\nabla^*Y_{\boldsymbol{\ell}}(\widehat{\boldsymbol{x}})| \leq C|\boldsymbol{\ell}|^{d/2}, \quad \widehat{\boldsymbol{x}} \in \mathbb{S}^{d-1}. \tag{2.25}$$

Substituting (2.18) and (2.19) in (2.23), yields the estimate

$$|\nabla\widetilde{E}_{\boldsymbol{\ell}}(\boldsymbol{x})| \leq C\left(\frac{\rho_D}{R}\right)^{|\boldsymbol{\ell}|-1}|\boldsymbol{\ell}|^{d/2-1} \qquad \forall \boldsymbol{\ell} \in \mathbb{I}_d,\ |\boldsymbol{\ell}| > 0,\ |\boldsymbol{x}| < R\,. \tag{2.26}$$

□

Using (2.15), we represent the incident wave u^{inc} as

$$u^{\text{inc}} = \sum_{\boldsymbol{\ell}\in\mathbb{I}_d} p_{\boldsymbol{\ell}}\widetilde{E}_{\boldsymbol{\ell}}. \tag{2.27}$$

Details of such expansions and weights for the physically important plane-wave and point-source incidence are discussed in § 3.1 and §3.2.

As with most error estimates, our truncation error bounds will depend on a measure of the "smoothness" of the data, which is expressed through requiring that suitable norms be bounded. Here, we assume that the incident wave $u^{\rm inc}$ with $u^{\rm inc}\restriction\partial D \in L^2(\partial D)$ is such that there exists a weight sequence $\boldsymbol{w} = (w_{\boldsymbol{\ell}})_{\boldsymbol{\ell}\in\mathbb{I}_d}$ with

$$0 < \underline{w} \le w_{\boldsymbol{\ell}} \quad \forall \boldsymbol{\ell} \in \mathbb{I}_d \quad \text{and some } \underline{w} > 0\,, \tag{2.28}$$

such that $u^{\rm inc} \in X_{\boldsymbol{w}}$, where

$$X_{\boldsymbol{w}} = \left\{ \psi = \sum_{\boldsymbol{\ell}\in\mathbb{I}_d} q_{\boldsymbol{\ell}} \widetilde{E}_{\boldsymbol{\ell}} : \|\psi\|^2_{X_{\boldsymbol{w}}} := \sum_{\boldsymbol{\ell}\in\mathbb{I}_d} w_{\boldsymbol{\ell}} |q_{\boldsymbol{\ell}}|^2 < \infty \right\}. \tag{2.29}$$

Remark 2.2 *Lemma 2.1 implies that for $u^{\rm inc} \in X_{\boldsymbol{w}}$ suitable restrictions of the expansion* (2.27) *converge in both $L^2(\partial D)$ and $L^2(B_R)$. From the estimates in the proof of Lemma 2.1 we also infer*

$$X_{\boldsymbol{w}}\restriction B_R \subset L^2(B_R) \quad \textit{with continuous embedding.} \tag{2.30}$$

We also introduce a new class of scaled radiating waves

$$E_{\boldsymbol{\ell}}(\boldsymbol{x}) = \begin{cases} \dfrac{\sqrt{\pi k}}{(-i)^{|\boldsymbol{\ell}|}(1-i)} H^{(1)}_{|\boldsymbol{\ell}|}(k|\boldsymbol{x}|) Y_{\boldsymbol{\ell}}(\widehat{\boldsymbol{x}}), & d = 2, \\ \dfrac{k}{(-i)^{|\ell|+1}} h^{(1)}_{|\boldsymbol{\ell}|}(k|\boldsymbol{x}|) Y_{\boldsymbol{\ell}}(\widehat{\boldsymbol{x}}), & d = 3, \end{cases} \qquad \boldsymbol{\ell} \in \mathbb{I}_d. \tag{2.31}$$

The scaling factors in (2.31) are applied to the usual outgoing wave functions so that their associated far-fields $\{E^\infty_{\boldsymbol{\ell}} : \boldsymbol{\ell} \in \mathbb{I}_d\}$ form an orthonormal basis for $L^2(\mathbb{S}^{d-1})$. In particular, using the asymptotics of the Hankel and spherical Hankel functions as $|\boldsymbol{x}| \to\infty$, see [4, Equations (3.59) and (2.41)], in (2.31) we get

$$E^\infty_{\boldsymbol{\ell}}(\widehat{\boldsymbol{x}}) = Y_{\boldsymbol{\ell}}(\widehat{\boldsymbol{x}}), \qquad \boldsymbol{\ell} \in \mathbb{I}_d,\ \widehat{\boldsymbol{x}} \in \mathbb{S}^{d-1},\ d = 2, 3. \tag{2.32}$$

Hence using (2.12),

$$u^\infty(\widehat{\boldsymbol{x}}) = \sum_{\boldsymbol{\ell}'\in\mathbb{I}_d} a_{\boldsymbol{\ell}'} E^\infty_{\boldsymbol{\ell}'}(\widehat{\boldsymbol{x}}), \qquad \widehat{\boldsymbol{x}} \in \mathbb{S}^{d-1}. \tag{2.33}$$

In view of the above, it is natural to represent the radiating scattered field $u^{\rm s}$ outside the ball B_R as

$$u^{\rm s}(\boldsymbol{x}) = \sum_{\boldsymbol{\ell}'\in\mathbb{I}_d} a_{\boldsymbol{\ell}'} E_{\boldsymbol{\ell}'}(\boldsymbol{x}), \qquad \boldsymbol{x} \in \mathbb{R}^d \setminus \overline{B}_R. \tag{2.34}$$

2.2 Infinite basis: scattering matrix, far-field, scattered-field

We introduce bounded linear operators $S_\partial^\infty : Z(\partial D) \to L^2(\mathbb{S}^{d-1})$, where

$$Z(\partial D) := \begin{cases} H^{1/2}(\partial D) & \text{for a sound-soft scatterer (2.2),} \\ L^2(\partial D) & \text{for boundary conditions (2.3), (2.4).} \end{cases}$$

These operators map boundary data $g \in Z(\partial D)$ to the far field pattern u^∞ of the solutions $u \in H^1_{\mathrm{loc}}(\mathbb{R}^d \setminus \overline{D})$ of the exterior boundary value problems[1]

$$\Delta u + k^2 u = 0 \quad \text{in } \mathbb{R}^d \setminus \overline{D}\,, \quad \begin{cases} u = g\,, & (2.35) \\ \textbf{or} & \\ \dfrac{\partial u}{\partial \boldsymbol{n}} = g\,, \quad \text{on } \partial D & (2.36) \\ \textbf{or} & \\ u + \lambda \dfrac{\partial u}{\partial \boldsymbol{n}} = g\,, & (2.37) \end{cases}$$

and Sommerfeld radiation condition (2.5) at infinity. Continuity of S_∂^∞ follows from the estimates in [4, Sect. 2.5] and the fact that $u \in H^1_{\mathrm{loc}}(\mathbb{R}^d \setminus \overline{B}_R)$. Using S_∂^∞ we define the scattered field operators $S^\infty : C^\infty(B_R) \mapsto L^2(\mathbb{S}^{d-1})$ as

$$S^\infty := S_\partial^\infty \circ B \quad , \quad B\psi := \begin{cases} \psi \restriction \partial D & \text{for (2.35)}\,, \\ \dfrac{\partial \psi}{\partial \boldsymbol{n}} \restriction \partial D & \text{for (2.36)}\,, \\ \psi + \lambda \dfrac{\partial \psi}{\partial \boldsymbol{n}} \restriction \partial D & \text{for (2.37)}\,. \end{cases} \tag{2.38}$$

Using (2.28) and the estimates of Lemma 2.1, we obtain that for u^{inc} the B-restrictions of the terms of the expansion (2.27) form sequences that converge in $Z(\partial D)$, which implies

$$S^\infty u^{\mathrm{inc}} = \sum_{\boldsymbol{\ell} \in \mathbb{I}_d} p_{\boldsymbol{\ell}} \left(S^\infty \widetilde{E}_{\boldsymbol{\ell}} \right) \quad \text{in } L^2(\mathbb{S}^{d-1})\,. \tag{2.39}$$

For each $\boldsymbol{\ell} \in \mathbb{I}_d$, since $S^\infty \widetilde{E}_{\boldsymbol{\ell}} \in L^2(\mathbb{S}^{d-1})$, there exist coefficients $t_{\boldsymbol{\ell}',\boldsymbol{\ell}}$ such that

$$\left(S^\infty \widetilde{E}_{\boldsymbol{\ell}} \right)(\widehat{\boldsymbol{x}}) = \sum_{\boldsymbol{\ell}' \in \mathbb{I}_d} t_{\boldsymbol{\ell}',\boldsymbol{\ell}} E^\infty_{\boldsymbol{\ell}'}(\widehat{\boldsymbol{x}}) = \sum_{\boldsymbol{\ell}' \in \mathbb{I}_d} t_{\boldsymbol{\ell}',\boldsymbol{\ell}} Y_{\boldsymbol{\ell}'}(\widehat{\boldsymbol{x}}), \qquad \widehat{\boldsymbol{x}} \in \mathbb{S}^{d-1}. \tag{2.40}$$

Using the orthonormality of the basis function in (2.10) with respect to the inner product $\langle \cdot, \cdot \rangle$ in $L^2(\mathbb{S}^{d-1})$, we get

$$t_{\boldsymbol{\ell}',\boldsymbol{\ell}} = \langle S^\infty \widetilde{E}_{\boldsymbol{\ell}}, Y_{\boldsymbol{\ell}'} \rangle, \qquad \boldsymbol{\ell}', \boldsymbol{\ell} \in \mathbb{I}_d. \tag{2.41}$$

[1] Of course, S_∂^∞ will be different for each boundary condition. For the sake of lean notations this dependence will be suppressed.

Using (2.40) in (2.39), we obtain

$$u^\infty(\widehat{\boldsymbol{x}}) = S^\infty u^{\rm inc}(\widehat{\boldsymbol{x}}) = \sum_{\boldsymbol{\ell}' \in \mathbb{I}_d} \left[\sum_{\boldsymbol{\ell} \in \mathbb{I}_d} t_{\boldsymbol{\ell}',\boldsymbol{\ell}} p_{\boldsymbol{\ell}} \right] E^\infty_{\boldsymbol{\ell}'}(\widehat{\boldsymbol{x}}), \qquad \widehat{\boldsymbol{x}} \in \mathbb{S}^{d-1}. \tag{2.42}$$

Comparing (2.42) with (2.33) shows that the incident field and the scattered/far-field coefficient sequences $\boldsymbol{p} = (p_{\boldsymbol{\ell}})_{\boldsymbol{\ell} \in \mathbb{I}_d}$ and $\boldsymbol{a} = (a_{\boldsymbol{\ell}})_{\boldsymbol{\ell} \in \mathbb{I}_d}$ are connected via the (infinite) T-matrix $T = \left[t_{\boldsymbol{\ell}',\boldsymbol{\ell}}\right]_{\boldsymbol{\ell}',\boldsymbol{\ell} \in \mathbb{I}_d}$ according to

$$\boldsymbol{a} = T\boldsymbol{p}. \tag{2.43}$$

2.3 Reduced basis: scattering matrix, far-field, scattered-field

For a fixed pair of truncation parameters $N', N \in \mathbb{N}$, using the representation (2.41), we define the truncated $N'_d \times N_d$ reduced basis acoustic scattering T-matrix as

$$T_{N',N} = \left[t_{\boldsymbol{\ell}',\boldsymbol{\ell}}\right]_{\boldsymbol{\ell}' \in \mathbb{I}_{d,N'}, \boldsymbol{\ell} \in \mathbb{I}_{d,N}}. \tag{2.44}$$

The $N'_d \times N_d$ truncated T-matrix can be precomputed and stored for any chosen scatterer, independent of the incident wave. Using the representation of $u^{\rm inc}$ in (2.27) and the associated truncated vector $\boldsymbol{p}^{(N)} = (p_{\boldsymbol{\ell}})_{\boldsymbol{\ell} \in \mathbb{I}_{d,N}}$ (which is known analytically for the physically important plane-wave and point-source incident waves), we can compute the vector $\boldsymbol{a}^{(N',N)} = \left(a^{(N',N)}_{\boldsymbol{\ell}'}\right)_{\boldsymbol{\ell}' \in \mathbb{I}'_{d,N}}$ using

$$\boldsymbol{a}^{(N',N)} = T_{N',N}\boldsymbol{p}^{(N)}. \tag{2.45}$$

In particular, using (2.33)–(2.42), for an incident field $u^{\rm inc}$ with representation (2.27), our approximation to the induced far-field is:

$$u^\infty_{(N',N)} = \sum_{\boldsymbol{\ell}' \in \mathbb{I}_{d,N'}} \left[\sum_{\boldsymbol{\ell} \in \mathbb{I}_{d,N}} t_{\boldsymbol{\ell}',\boldsymbol{\ell}} p_{\boldsymbol{\ell}} \right] E^\infty_{\boldsymbol{\ell}'} = \sum_{\boldsymbol{\ell}' \in \mathbb{I}_{d,N'}} \left[\sum_{\boldsymbol{\ell} \in \mathbb{I}_{d,N}} t_{\boldsymbol{\ell}',\boldsymbol{\ell}} p_{\boldsymbol{\ell}} \right] Y_{\boldsymbol{\ell}'}. \tag{2.46}$$

Our approximation to the scattered field in (2.34) is $u^{\rm s}_{(N',N)}$, which is computed similarly, using the T-matrix with $E^\infty_{\boldsymbol{\ell}'}$ in (2.46) replaced with $E_{\boldsymbol{\ell}'}$.

3 Convergence analysis with parameter estimates

In this section we prove that $u^\infty_{(N',N)}$ converges exponentially to u^∞ in $L^2(\mathbb{S}^{d-1})$ with respect to the truncation parameters N, N'.

Lemma 3.1 *Let $u^{\rm inc} \in X_{\boldsymbol{w}}$. Then*

$$\begin{aligned} &\left\|u^\infty - u^\infty_{(N',N)}\right\|^2_{L^2(\mathbb{S}^{d-1})} \\ \leq\ &\left\|u^{\rm inc}\right\|^2_{X_{\boldsymbol{w}}} \left\{ \sum_{\boldsymbol{\ell} \in \mathbb{I}_d} \frac{1}{w_{\boldsymbol{\ell}}} \left\| S^\infty \widetilde{E}_{\boldsymbol{\ell}} - S^\infty_{N'} \widetilde{E}_{\boldsymbol{\ell}} \right\|^2_{L^2(\mathbb{S}^{d-1})} + \sum_{\boldsymbol{\ell} \in \mathbb{I}_d \setminus \mathbb{I}_{d,N}} \frac{1}{w_{\boldsymbol{\ell}}} \left\| S^\infty \widetilde{E}_{\boldsymbol{\ell}} \right\|^2_{L^2(\mathbb{S}^{d-1})} \right\}, \end{aligned} \tag{3.1}$$

where $S^\infty_{N'} \widetilde{E}_{\boldsymbol{\ell}}$ is the $L^2(\mathbb{S}^{d-1})$-orthogonal projection of $S^\infty \widetilde{E}_{\boldsymbol{\ell}}$ onto $\operatorname{span}\{Y_{\boldsymbol{\ell}'} : \boldsymbol{\ell}' \in \mathbb{I}_{d,N'}\}$.

Proof. Using (2.42) and (2.46),

$$u^\infty - u^\infty_{(N',N)} = \sum_{\boldsymbol{\ell}' \in \mathbb{I}_d \setminus \mathbb{I}_{d,N'}} \left[\sum_{\boldsymbol{\ell} \in \mathbb{I}_d} t_{\boldsymbol{\ell}',\boldsymbol{\ell}} p_{\boldsymbol{\ell}} \right] Y_{\boldsymbol{\ell}'} + \sum_{\boldsymbol{\ell}' \in \mathbb{I}_{d,N'}} \left[\sum_{\boldsymbol{\ell} \in \mathbb{I}_d \setminus \mathbb{I}_{d,N}} t_{\boldsymbol{\ell}',\boldsymbol{\ell}} p_{\boldsymbol{\ell}} \right] Y_{\boldsymbol{\ell}'}. \tag{3.2}$$

Hence, by the orthonormality of the basis functions $Y_{\boldsymbol{\ell}'}$ of $L^2(\mathbb{S}^{d-1})$,

$$\left\| u^\infty - u^\infty_{(N',N)} \right\|^2_{L^2(\mathbb{S}^{d-1})} = \sum_{\boldsymbol{\ell}' \in \mathbb{I}_d \setminus \mathbb{I}_{d,N'}} \left| \sum_{\boldsymbol{\ell} \in \mathbb{I}_d} \frac{t_{\boldsymbol{\ell}',\boldsymbol{\ell}}}{\sqrt{w_{\boldsymbol{\ell}}}} \sqrt{w_{\boldsymbol{\ell}}} p_{\boldsymbol{\ell}} \right|^2 + \sum_{\boldsymbol{\ell}' \in \mathbb{I}_{d,N'}} \left| \sum_{\boldsymbol{\ell} \in \mathbb{I}_d \setminus \mathbb{I}_{d,N}} \frac{t_{\boldsymbol{\ell}',\boldsymbol{\ell}}}{\sqrt{w_{\boldsymbol{\ell}}}} \sqrt{w_{\boldsymbol{\ell}}} p_{\boldsymbol{\ell}} \right|^2. \tag{3.3}$$

Hence the Cauchy-Schwarz inequality and (2.27) yield

$$\begin{aligned}
\left\| u^\infty - u^\infty_{(N',N)} \right\|^2_{L^2(\mathbb{S}^{d-1})} &\leq \left\| u^{\mathrm{inc}} \right\|^2_{X_{\boldsymbol{w}}} \left[\sum_{\boldsymbol{\ell}' \in \mathbb{I}_d \setminus \mathbb{I}_{d,N'}} \sum_{\boldsymbol{\ell} \in \mathbb{I}_d} \frac{|t_{\boldsymbol{\ell}',\boldsymbol{\ell}}|^2}{w_{\boldsymbol{\ell}}} + \sum_{\boldsymbol{\ell}' \in \mathbb{I}_{d,N'}} \sum_{\boldsymbol{\ell} \in \mathbb{I}_d \setminus \mathbb{I}_{d,N}} \frac{|t_{\boldsymbol{\ell}',\boldsymbol{\ell}}|^2}{w_{\boldsymbol{\ell}}} \right] \\
&= \left\| u^{\mathrm{inc}} \right\|^2_{X_{\boldsymbol{w}}} \left[\sum_{\boldsymbol{\ell} \in \mathbb{I}_d} \frac{1}{w_{\boldsymbol{\ell}}} \sum_{\boldsymbol{\ell}' \in \mathbb{I}_d \setminus \mathbb{I}_{d,N'}} |t_{\boldsymbol{\ell}',\boldsymbol{\ell}}|^2 + \sum_{\boldsymbol{\ell} \in \mathbb{I}_d \setminus \mathbb{I}_{d,N}} \frac{1}{w_{\boldsymbol{\ell}}} \sum_{\boldsymbol{\ell}' \in \mathbb{I}_d} |t_{\boldsymbol{\ell}',\boldsymbol{\ell}}|^2 \right] \\
&= \left\| u^{\mathrm{inc}} \right\|^2_{X_{\boldsymbol{w}}} \left[\sum_{\boldsymbol{\ell} \in \mathbb{I}_d} \frac{1}{w_{\boldsymbol{\ell}}} \sum_{\boldsymbol{\ell}' \in \mathbb{I}_d \setminus \mathbb{I}_{d,N'}} |t_{\boldsymbol{\ell}',\boldsymbol{\ell}}|^2 + \sum_{\boldsymbol{\ell} \in \mathbb{I}_d \setminus \mathbb{I}_{d,N}} \frac{1}{w_{\boldsymbol{\ell}}} \left\| S^\infty \widetilde{E}_{\boldsymbol{\ell}} \right\|^2_{L^2(\mathbb{S}^{d-1})} \right],
\end{aligned}$$

where in the last line we used (2.40). Now the result (3.1) follows from using

$$\left(S^\infty_{N'} \widetilde{E}_{\boldsymbol{\ell}} \right)(\widehat{\boldsymbol{x}}) = \sum_{\boldsymbol{\ell}' \in \mathbb{I}_{d,N'}} t_{\boldsymbol{\ell}',\boldsymbol{\ell}} Y_{\boldsymbol{\ell}'}(\widehat{\boldsymbol{x}}), \qquad \widehat{\boldsymbol{x}} \in \mathbb{S}^{d-1}, \tag{3.4}$$

and the identity

$$\left\| S^\infty \widetilde{E}_{\boldsymbol{\ell}} - S^\infty_{N'} \widetilde{E}_{\boldsymbol{\ell}} \right\|^2_{L^2(\mathbb{S}^{d-1})} = \sum_{\boldsymbol{\ell}' \in \mathbb{I}_d \setminus \mathbb{I}_{d,N'}} |t_{\boldsymbol{\ell}',\boldsymbol{\ell}}|^2. \tag{3.5}$$

□

Next we estimate the first term in (3.1). We recall that ρ_D is the radius of the scatterer D, that $R > \rho_D$ is fixed, and that k is the wavenumber of the obstacle scattering problem.

Lemma 3.2 *The restrictions of the incident base fields from* (2.15) *satisfy*

$$\left\| \widetilde{E}_{\boldsymbol{\ell}} \restriction \partial D \right\|_{Z(\partial D)} \leq C \left(\frac{\rho_D}{R} \right)^{|\boldsymbol{\ell}|} \cdot \begin{cases} |\boldsymbol{\ell}|^{d/4 - 1/2}, & \textit{for sound-soft scatterer,} \\ 1, & \textit{for boundary conditions } (2.3),\ (2.4). \end{cases}$$

Proof. The estimate is an immediate consequence of the bounds (2.16) and (2.17) from Lemma 2.1 and the standard interpolation estimate $\|u\|_{H^{1/2}(\partial D)} \leq C \|u\|^{1/2}_{H^1(\partial D)} \|u\|^{1/2}_{L^2(\partial D)}$. □

Lemma 3.3 *For all $\boldsymbol{\ell} \in \mathbb{I}_d$, and assuming the threshold condition $N' > Rk/2$, we have the estimate*

$$\left\| S^\infty \widetilde{E}_{\boldsymbol{\ell}} - S^\infty_{N'} \widetilde{E}_{\boldsymbol{\ell}} \right\|^2_{L^2(\mathbb{S}^{d-1})} = \sum_{\boldsymbol{\ell}' \in \mathbb{I}_d \setminus \mathbb{I}_{d,N'}} |t_{\boldsymbol{\ell}',\boldsymbol{\ell}}|^2 \leq C \left(\frac{Rke}{2N'} \right)^{2N'} \left(\frac{\rho_D}{R} \right)^{2|\boldsymbol{\ell}|} |\boldsymbol{\ell}|^{d/2-1} . \tag{3.6}$$

Proof. We introduce the operators $S_R : Z(\partial D) \mapsto L^2(\partial B_R)$, $S_R g := u\restriction \partial B_R$, where $u \in H^1_{\mathrm{loc}}(\mathbb{R}^d \setminus \overline{\Omega})$ is the solution of one of the exterior boundary value problems from (2.35)–(2.37). Obviously, S_R is a *bounded* linear operator. We denote by $\|S_R\|$ the norm of S_R as a mapping $Z(\partial D) \mapsto L^2(\partial B_R)$. This norm may be incorporated into constants, whenever appropriate.

Following the considerations in [4, Sect. 2.5] (for $d = 3$) and [12, Section 4] (for $d = 2$), we find that the coefficients $a_{\boldsymbol{\ell}'}$ of the expansion (2.12) of u^∞, which is the far field pattern of the solution u induced by the boundary data g, satisfy

$$\sum_{\boldsymbol{\ell}' \in \mathbb{I}_d} \left(\frac{2|\boldsymbol{\ell}'|}{Rke} \right)^{2|\boldsymbol{\ell}'|} |a_{\boldsymbol{\ell}'}|^2 \leq C(Rk)^{1-d} \|u\|^2_{L^2(\partial B_R)} \leq C(Rk)^{1-d} \|S_R\| \, \|g\|_{Z(\partial D)} . \tag{3.7}$$

Thus, defining the Hilbert space

$$Y_R = \left\{ \psi = \sum_{\boldsymbol{\ell}' \in \mathbb{I}_d} g_{\boldsymbol{\ell}'} Y_{\boldsymbol{\ell}'} : \sum_{\boldsymbol{\ell}' \in \mathbb{I}_d} \left(\frac{2|\boldsymbol{\ell}'|}{Rke} \right)^{2|\boldsymbol{\ell}'|} |g_{\boldsymbol{\ell}'}|^2 < \infty \right\} \subset L^2(\mathbb{S}^{d-1}), \tag{3.8}$$

equipped with norm $\|\psi\|^2_{Y_R} = \sum_{\boldsymbol{\ell}' \in \mathbb{I}_d} \left(\frac{2|\boldsymbol{\ell}'|}{Rke} \right)^{2|\boldsymbol{\ell}'|} |g_{\boldsymbol{\ell}}|^2$, we find that $S^\infty_\partial : Z(\partial D) \to Y_R$ is a bounded linear operator. Note that the $t_{\boldsymbol{\ell}',\boldsymbol{\ell}}$ are the expansion coefficients of $S^\infty \widetilde{E}_{\boldsymbol{\ell}}$. Consequently, using (3.5),

$$\begin{aligned} \left\| S^\infty \widetilde{E}_{\boldsymbol{\ell}} - S^\infty_{N'} \widetilde{E}_{\boldsymbol{\ell}} \right\|^2_{L^2(\mathbb{S}^{d-1})} &= \sum_{\boldsymbol{\ell}' \in \mathbb{I}_d \setminus \mathbb{I}_{d,N'}} |t_{\boldsymbol{\ell}',\boldsymbol{\ell}}|^2 \\ &= \sum_{\boldsymbol{\ell}' \in \mathbb{I}_d \setminus \mathbb{I}_{d,N'}} \left(\frac{Rke}{2|\boldsymbol{\ell}'|} \right)^{2|\boldsymbol{\ell}'|} \left(\frac{2|\boldsymbol{\ell}'|}{Rke} \right)^{2|\boldsymbol{\ell}'|} |t_{\boldsymbol{\ell}',\boldsymbol{\ell}}|^2 \\ &= \sum_{\boldsymbol{\ell}' \in \mathbb{I}_d \setminus \mathbb{I}_{d,N'}} f_{Rke}(2|\boldsymbol{\ell}'|) \left(\frac{2|\boldsymbol{\ell}'|}{Rke} \right)^{2|\boldsymbol{\ell}'|} |t_{\boldsymbol{\ell}',\boldsymbol{\ell}}|^2, \end{aligned} \tag{3.9}$$

where for a fixed $a > 0$,

$$f_a(x) = (a/x)^x , \qquad x > 0. \tag{3.10}$$

It is easy to check that $\lim_{x\to 0} f_a(x) = 1$, that $\lim_{x\to\infty} f_a(x) = 0$, that $f_a(x)$ attains its maximum at $x^* = a/e$, and that $f_a(x)$ is a decreasing function for $x > x^*$. Using these

properties in (3.9), for $N' > Rk/2$,

$$\begin{aligned}
\left\| S^\infty \widetilde{E}_{\boldsymbol{\ell}} - S^\infty_{N'} \widetilde{E}_{\boldsymbol{\ell}} \right\|^2_{L^2(\mathbb{S}^{d-1})} &\leq \left(\frac{Rke}{2N'}\right)^{2N'} \sum_{\boldsymbol{\ell}' \in \mathbb{I}_d \setminus \mathbb{I}_{d,N'}} \left(\frac{2|\boldsymbol{\ell}'|}{Rke}\right)^{2|\boldsymbol{\ell}'|} |t_{\boldsymbol{\ell}',\boldsymbol{\ell}}|^2 \\
&\leq \left(\frac{Rke}{2N'}\right)^{2N'} \left\| S^\infty \widetilde{E}_{\boldsymbol{\ell}} \right\|^2_{Y_R} \\
&\leq C \left(\frac{Rke}{2N'}\right)^{2N'} C \left\| S_R \right\| \left\| \widetilde{E}_{\boldsymbol{\ell}} \right\|^2_{Z(\partial D)} \\
&\leq C \left\| S_R \right\| \left(\frac{Rke}{2N'}\right)^{2N'} \left(\frac{\rho_D}{R}\right)^{2|\boldsymbol{\ell}|} |\boldsymbol{\ell}|^{d/2-1} .
\end{aligned}$$

where in the last step we invoked the estimates Lemma 3.2 and used a common upper bound. □

Lemma 3.4 *For all $R > \rho_D$ and $\boldsymbol{\ell} \in \mathbb{I}_d$,*

$$\left\| S^\infty \widetilde{E}_{\boldsymbol{\ell}} \right\|^2_{L^2(\mathbb{S}^{d-1})} \leq C \left(\frac{\rho_D}{R}\right)^{2|\boldsymbol{\ell}|} |\boldsymbol{\ell}|^{d/2-1}. \tag{3.11}$$

Proof. Appealing to the continuity of $S^\infty_\partial : Z(\partial D) \mapsto L^2(\mathbb{S}^{d-1})$, the estimate is immediate from Lemma 3.2. □

Using (3.6) and (3.11) in (3.1), we get the following result.

Theorem 3.5 *Let $u^{\rm inc} \in X_{\boldsymbol{w}}$. Assuming the threshold condition $N' > Rk/2$, there holds*

$$\begin{aligned}
&\left\| u^\infty - u^\infty_{(N',N)} \right\|^2_{L^2(\mathbb{S}^{d-1})} \\
\leq\ & C \left\| u^{\rm inc} \right\|^2_{X_{\boldsymbol{w}}} \left\{ \left(\frac{Rke}{2N'}\right)^{2N'} \sum_{\boldsymbol{\ell} \in \mathbb{I}_d} \frac{|\boldsymbol{\ell}|^{d/2-1}}{w_{\boldsymbol{\ell}}} \left(\frac{\rho_D}{R}\right)^{2|\boldsymbol{\ell}|} + \sum_{\boldsymbol{\ell} \in \mathbb{I}_d \setminus \mathbb{I}_{d,N}} \frac{|\boldsymbol{\ell}|^{d/2-1}}{w_{\boldsymbol{\ell}}} \left(\frac{\rho_D}{R}\right)^{2|\boldsymbol{\ell}|} \right\} .
\end{aligned} \tag{3.12}$$

3.1 Convergence analysis for plane-wave incidence

Let $u^{\rm inc}(\boldsymbol{x}) = \exp(ik\boldsymbol{x} \cdot \widehat{\boldsymbol{d}})$ be the plane-wave with fixed incident direction $\widehat{\boldsymbol{d}}$ impinging on the obstacle $D \in \mathbb{R}^d$ for $d = 2, 3$. The expansion coefficients of the incident wave in the expansion (2.27) are [4, Equation (3.66) for $d = 2$ and Equation (2.45) for $d = 3$]

$$p_{\boldsymbol{\ell}} = \begin{cases} \sqrt{2\pi} \dfrac{i^{|\boldsymbol{\ell}|}}{H^{(1)}_{\boldsymbol{\ell}}(kR)} \overline{Y_{\boldsymbol{\ell}}(\widehat{\boldsymbol{d}})}, & \text{for } d = 2, \\ 4\pi \dfrac{i^{|\boldsymbol{\ell}|}}{h^{(1)}_{\boldsymbol{\ell}}(kR)} \overline{Y_{\boldsymbol{\ell}}(\widehat{\boldsymbol{d}})}, & \text{for } d = 3. \end{cases} \tag{3.13}$$

From (2.20), it is easy to see that the coefficients $p_{\boldsymbol{\ell}}$ satisfy the decay bound

$$|p_{\boldsymbol{\ell}}| \leq C \cdot \begin{cases} \dfrac{1}{H^{(1)}_{|\boldsymbol{\ell}|}(kR)}, & \text{for } d = 2, \\ \dfrac{|\boldsymbol{\ell}|^{1/2}}{h^{(1)}_{|\boldsymbol{\ell}|}(kR)}, & \text{for } d = 3, \end{cases} \qquad \boldsymbol{\ell} \in \mathbb{I}_d. \tag{3.14}$$

Hence using the asymptotics of the Hankel and spherical Hankel functions for $|\boldsymbol{\ell}| \to \infty$ [4, Equations (3.58) and (2.39)], if we choose (see Figure 2)

$$w_{\boldsymbol{\ell}} = |\boldsymbol{\ell}|^{-d} \left(\frac{2|\boldsymbol{\ell}|}{Rke} \right)^{2|\boldsymbol{\ell}|}, \tag{3.15}$$

it is easy to see that $u^{\text{inc}} \in X_{\boldsymbol{w}}$. Also

$$\frac{|\boldsymbol{\ell}|^{d/2-1}}{w_{\boldsymbol{\ell}}} \left(\frac{\rho_D}{R} \right)^{2|\boldsymbol{\ell}|} = |\boldsymbol{\ell}|^{3d/2-1} \left(\frac{\rho_D ke}{2|\boldsymbol{\ell}|} \right)^{2|\boldsymbol{\ell}|} = g_{Rke}^{3d/2-1}(2|\boldsymbol{\ell}|) \left(\frac{\rho_D}{R} \right)^{2|\boldsymbol{\ell}|} \tag{3.16}$$

with

$$g_a^p(x) = \left(\frac{x}{2} \right)^p \left(\frac{a}{x} \right)^x, \qquad a, p > 0. \tag{3.17}$$

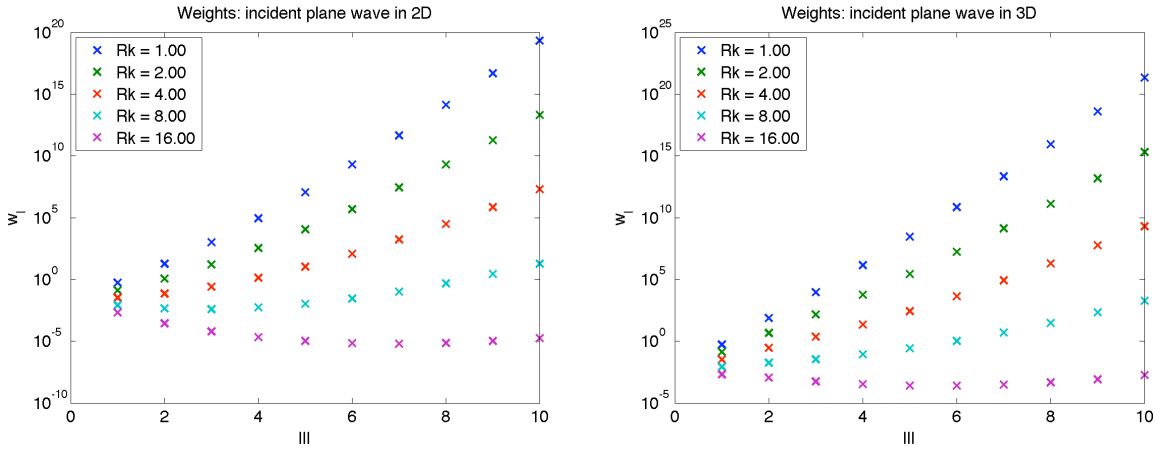

Figure 2: Weights $w_{\boldsymbol{\ell}}$ from (3.15).

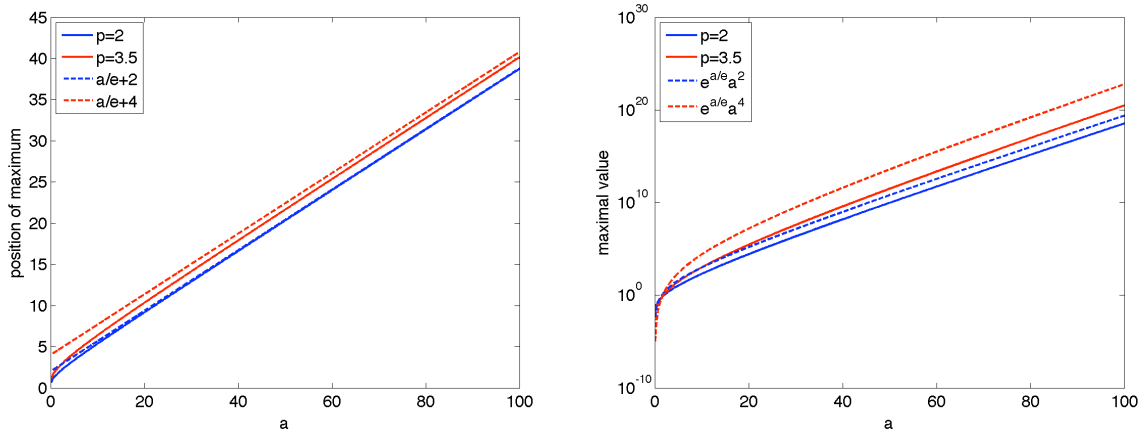

Figure 3: $x^*(p, a)$ (left) and $g_a^p(x^*)$ (right) as functions of a for relevant cases $p = 2, 3.5$.

If we write $g_a^p(x) = \exp(\varphi(x))$, we see that that the derivative $\varphi'(x)$ is a strictly decreasing function with $\varphi'(\frac{a}{e}) = \frac{ap}{e} > 0$ and $\varphi'(\frac{a}{e}+p) < 0$. Hence $g_a^p(x)$ has a single global maximum at $x^*(a,p)$ with $x^*(a,p) \le \frac{a}{e}+p$ (see Fig 3). Thus, we obtain for $N > Rk/2 + \frac{3d}{4} - \frac{1}{2}$

$$\sum_{\boldsymbol{\ell}\in\mathbb{I}_d\setminus\mathbb{I}_{d,N}} \frac{|\boldsymbol{\ell}|^{d/2-1}}{w_{\boldsymbol{\ell}}} \left(\frac{\rho_D}{R}\right)^{2|\boldsymbol{\ell}|} \le g_{Rke}^{3d/2-1}(2N) \sum_{\boldsymbol{\ell}\in\mathbb{I}_d\setminus\mathbb{I}_{d,N}} \left(\frac{\rho_D}{R}\right)^{2|\boldsymbol{\ell}|} \le CN^{3d/2-1} \left(\frac{Rke}{2N}\right)^{2N} \left(\frac{\rho_D}{R}\right)^{2N}. \tag{3.18}$$

The function $\varphi(x)$ introduced above is concave, increasing for $x \le \frac{a}{e}$ and decreasing for $x \ge \frac{a}{e}+p$. It can be bounded by the minimum of the tangent lines at these two sites, which leads to the estimate $g_a^p(x) \le (a/2)^p \exp(\frac{a}{e})$, *cf.* Figure 3. From it we conclude

$$\begin{aligned}\sum_{\boldsymbol{\ell}\in\mathbb{I}_d} \frac{|\boldsymbol{\ell}|^{d/2-1}}{w_{\boldsymbol{\ell}}} \left(\frac{\rho_D}{R}\right)^{2|\boldsymbol{\ell}|} &= \sum_{\boldsymbol{\ell}\in\mathbb{I}_d} g_{Rke}^{3d/2-1}(2|\boldsymbol{\ell}|) \left(\frac{\rho_D}{R}\right)^{2|\boldsymbol{\ell}|} \\ &\le e^{Rk}(Rke/2)^{3d/2-1} \sum_{\boldsymbol{\ell}\in\mathbb{I}_d} \left(\frac{\rho_D}{R}\right)^{2|\boldsymbol{\ell}|} \le Ce^{Rk}(Rke/2)^{3d/2-1}. \end{aligned} \tag{3.19}$$

Using (3.16), (3.18) and (3.19) in (3.12), we get the following exponential convergence of the far-field obtained using the truncated T-matrix $T_{N',N}$.

Theorem 3.6 *Let $u^{\rm inc}(\boldsymbol{x}) = \exp(ik\boldsymbol{x}\cdot\widehat{\boldsymbol{d}})$, $\widehat{\boldsymbol{d}} \in \mathbb{S}^{d-1}$ for $d = 2, 3$. If the threshold conditions $N' > Rk/2$ and $N > Rk/2 + \frac{3d}{4} - \frac{1}{2}$ are satisfied, there holds the estimate*

$$\left\|u^\infty - u^\infty_{(N',N)}\right\|^2_{L^2(\mathbb{S}^{d-1})} \le C\left\{e^{Rk}(Rke/2)^{3d/2-1}\left(\frac{Rke}{2N'}\right)^{2N'} + N^{3d/2-1}\left(\frac{\rho_D ke}{2N}\right)^{2N}\right\}. \tag{3.20}$$

3.2 Convergence analysis for point-source incidence

Let $\boldsymbol{x}_0 \in \mathbb{R}^d$ for $d = 2, 3$ with $|\boldsymbol{x}_0| > R$. Consider the incident field created by a point-source located at $\boldsymbol{x}_0$, that is,

$$u^{\rm inc}(\boldsymbol{x}) = \begin{cases} H_0^{(1)}(k|\boldsymbol{x}-\boldsymbol{x}_0|), & d = 2, \\ \dfrac{\exp(ik|\boldsymbol{x}-\boldsymbol{x}_0|)}{k|\boldsymbol{x}-\boldsymbol{x}_0|}, & d = 3. \end{cases} \tag{3.21}$$

The expansion coefficients of the incident wave in the expansion (2.27) are [4, Equation (3.65) for $d = 2$ and Equation (2.42) for $d = 3$]

$$p_{\boldsymbol{\ell}} = \begin{cases} \sqrt{2\pi}\dfrac{H_{|\boldsymbol{\ell}|}^{(1)}(k|\boldsymbol{x}_0|)}{H_{|\boldsymbol{\ell}|}^{(1)}(kR)}\overline{Y_{\boldsymbol{\ell}}(\widehat{\boldsymbol{x}}_0)}, & \text{for } d = 2, \\ 4\pi ik\dfrac{h_{|\ell|}^{(1)}(k|\boldsymbol{x}_0|)}{h_{|\boldsymbol{\ell}|}^{(1)}(kR)}\overline{Y_{\boldsymbol{\ell}}(\widehat{\boldsymbol{x}}_0)}, & \text{for } d = 3, \end{cases} \qquad \boldsymbol{\ell} \in \mathbb{I}_d. \tag{3.22}$$

By (2.20) it is easy to see that the coefficients $p_{\boldsymbol{\ell}}$ satisfy the decay bounds

$$|p_{\boldsymbol{\ell}}| \le C \begin{cases} \left| \dfrac{H^{(1)}_{|\boldsymbol{\ell}|}(k|\boldsymbol{x}_0|)}{H^{(1)}_{|\boldsymbol{\ell}|}(kR)} \right| , & \text{for } d=2, \\ \\ |\boldsymbol{\ell}|^{1/2} \left| \dfrac{h^{(1)}_{|\boldsymbol{\ell}|}(k|\boldsymbol{x}_0|)}{h^{(1)}_{|\boldsymbol{\ell}|}(kR)} \right|, & \text{for } d=3, \end{cases} \qquad \boldsymbol{\ell} \in \mathbb{I}_d. \tag{3.23}$$

Hence, using the asymptotics of the Hankel and spherical Hankel functions for $|\boldsymbol{\ell}| \to \infty$ we arrive at the bound

$$|p_{\boldsymbol{\ell}}| \le C|\boldsymbol{\ell}|^{d/2-1} \left(\frac{R}{|\boldsymbol{x}_0|} \right)^{|\boldsymbol{\ell}|}, \quad \boldsymbol{\ell} \in \mathbb{I}_d \, . \tag{3.24}$$

Thus, if we choose $w_0 := 1$ and

$$w_{\boldsymbol{\ell}} := \frac{1}{|\boldsymbol{\ell}|^d} \left(\frac{|\boldsymbol{x}_0|}{R} \right)^{2|\boldsymbol{\ell}|}, \qquad \boldsymbol{\ell} \in \mathbb{I}_d, \ |\boldsymbol{\ell}| > 0 \, , \tag{3.25}$$

it is easy to see that $u^{\rm inc} \in X_{\boldsymbol{w}}$ with $\left\| u^{\rm inc} \right\|_{X_{\boldsymbol{w}}}$ bounded uniformly in $\boldsymbol{x}_0$ and k. In addition

$$\frac{1}{w_{\boldsymbol{\ell}}} \left(\frac{\rho_D}{R} \right)^{2|\boldsymbol{\ell}|} |\boldsymbol{\ell}|^{d/2-1} = |\boldsymbol{\ell}|^{3d/2-1} \left(\frac{\rho_D}{|\boldsymbol{x}_0|} \right)^{2|\boldsymbol{\ell}|} , \tag{3.26}$$

which, using bounds for sums of the form $\sum\limits_{k=N}^{\infty} k^p q^k$, $|q| < 1$, provides the estimates ($N > 1$)

$$\sum_{\boldsymbol{\ell} \in \mathbb{I}_d \setminus \mathbb{I}_{d,N}} \frac{1}{w_{\boldsymbol{\ell}}} \left(\frac{\rho_D}{R} \right)^{2|\boldsymbol{\ell}|} |\boldsymbol{\ell}|^{d/2-1} \le C \left(\frac{\rho_D}{|\boldsymbol{x}_0|} \right)^{2N} \cdot \begin{cases} \dfrac{N^2}{(1-(\rho_D/|\boldsymbol{x}_0|)^2)^3} & \text{for } d=2 \, , \\ \dfrac{N^{4.5}}{(1-(\rho_D/|\boldsymbol{x}_0|)^2)^{5.5}} & \text{for } d=3 \, . \end{cases} \tag{3.27}$$

Using (3.27) and $\rho_D < R < |\boldsymbol{x}_0|$ in (3.12) in Theorem 3.5, we get the following exponential convergence of the far-field approximation obtained using the truncated T-matrix $T_{N',N}$.

Theorem 3.7 *Let $u^{\rm inc}$ be as in (3.21) with $|x_0| > R$. Under the threshold condition $N' > Rk/2$,*

$$\left\| u^{\infty} - u^{\infty}_{(N',N)} \right\|^2_{L^2(\mathbb{S}^{d-1})} \le \frac{C}{(1-(\rho_D/|\boldsymbol{x}_0|)^2)^{q+1}} \cdot \left\{ \left(\frac{Rke}{2N'} \right)^{2N'} + N^q \left(\frac{\rho_D}{|\boldsymbol{x}_0|} \right)^{2N} \right\} , \tag{3.28}$$

with $q = 2$ for $d = 2$, and $q = 4.5$ for $d = 3$.

Note that the inevitable blow-up as the point source approaches D is reflected in the estimate (3.28).

3.3 Convergence analysis with approximate far-fields

The analysis above is based on the assumption that the far-field $S^\infty \widetilde{E}_{\boldsymbol{\ell}}$ required to construct entries $t_{\boldsymbol{\ell}',\boldsymbol{\ell}}$ for $\boldsymbol{\ell}' \in \mathbb{I}_{d,N'}$ and $\boldsymbol{\ell} \in \mathbb{I}_{d,N}$ in (2.41) for the reduced basis T-matrix can computed exactly. In practice, computation of $S^\infty \widetilde{E}_{\boldsymbol{\ell}}$ requires numerical algorithms to solve (offline) the wave propagation model (2.1)–(2.5) with $u^{\rm inc} = \widetilde{E}_{\boldsymbol{\ell}}$. In our approach any numerical method (such as finite element, boundary element, spectral, or fundamental solution) can be used to solve the model. Let $0 < \epsilon(\boldsymbol{\ell}) < 1$ be the relative approximation error in the numerically computed far-field with $u^{\rm inc} = \widetilde{E}_{\boldsymbol{\ell}},\ \boldsymbol{\ell} \in \mathbb{I}_{d,N}$. That is, we assume that the numerical method is such that the numerical far-field $S_h^\infty \widetilde{E}_{\boldsymbol{\ell}}$ approximating $S^\infty \widetilde{E}_{\boldsymbol{\ell}}$ satisfies

$$\left\| S_h^\infty \widetilde{E}_{\boldsymbol{\ell}} - S^\infty \widetilde{E}_{\boldsymbol{\ell}} \right\|_{L^2(\mathbb{S}^{d-1})} \leq \epsilon(\boldsymbol{\ell}) \leq \epsilon\ , \quad \boldsymbol{\ell} \in \mathbb{I}_{d,N}\ . \tag{3.29}$$

Different S_h^∞ may be employed for different incident fields $\widetilde{E}_{\boldsymbol{\ell}}$, to obtain a fixed accuracy $0 < \epsilon < 1$ so that $\epsilon(\boldsymbol{\ell}) \leq \epsilon,\ \boldsymbol{\ell} \in \mathbb{I}_{d,N}$.

Let $t_{\boldsymbol{\ell}',\boldsymbol{\ell},h}$ and $u^\infty_{(N',N,h)}$, respectively, be the associated approximations to $t_{\boldsymbol{\ell}',\boldsymbol{\ell}}$ and $u^\infty_{(N',N)}$. That is, based on (2.41) and (2.46), we have

$$t_{\boldsymbol{\ell}',\boldsymbol{\ell}} = \langle S^\infty \widetilde{E}_{\boldsymbol{\ell}}, Y_{\boldsymbol{\ell}'} \rangle, \qquad t_{\boldsymbol{\ell}',\boldsymbol{\ell},h} = \langle S_h^\infty \widetilde{E}_{\boldsymbol{\ell}}, Y_{\boldsymbol{\ell}'} \rangle, \qquad \boldsymbol{\ell}' \in \mathbb{I}_{d,N'}, \boldsymbol{\ell} \in \mathbb{I}_{d,N}. \tag{3.30}$$

$$u^\infty_{(N',N)} = \sum_{\boldsymbol{\ell}' \in \mathbb{I}_{d,N'}} \left[\sum_{\boldsymbol{\ell} \in \mathbb{I}_{d,N}} t_{\boldsymbol{\ell}',\boldsymbol{\ell}} p_{\boldsymbol{\ell}} \right] Y_{\boldsymbol{\ell}'}, \qquad u^\infty_{(N',N,h)} = \sum_{\boldsymbol{\ell}' \in \mathbb{I}_{d,N'}} \left[\sum_{\boldsymbol{\ell} \in \mathbb{I}_{d,N}} t_{\boldsymbol{\ell}',\boldsymbol{\ell},h} p_{\boldsymbol{\ell}} \right] Y_{\boldsymbol{\ell}'}. \tag{3.31}$$

Using (3.30) and (3.29) we get

$$\sum_{\boldsymbol{\ell}' \in \mathbb{I}_{d,N'}} \left| t_{\boldsymbol{\ell}',\boldsymbol{\ell},h} - t_{\boldsymbol{\ell}',\boldsymbol{\ell}} \right|^2 \leq \sum_{\boldsymbol{\ell}' \in \mathbb{I}_{d,N'}} \left| \langle (S_h^\infty - S^\infty)\, \widetilde{E}_{\boldsymbol{\ell}}, Y_{\boldsymbol{\ell}'} \rangle \right|^2 = \epsilon(\boldsymbol{\ell})^2\ . \tag{3.32}$$

Again using the $L^2(\mathbb{S}^{d-1})$-orthonormality of the $Y_{\boldsymbol{\ell}'}$, (3.31) and (3.32), we get

$$\begin{aligned} \left\| u^\infty_{(N',N,h)} - u^\infty_{(N',N)} \right\|^2_{L^2(\mathbb{S}^{d-1})} &\leq \sum_{\boldsymbol{\ell} \in \mathbb{I}_{d,N}} \sum_{\boldsymbol{\ell}' \in \mathbb{I}_{d,N'}} \left| t_{\boldsymbol{\ell}',\boldsymbol{\ell},h} - t_{\boldsymbol{\ell}',\boldsymbol{\ell}} \right|^2 |p_{\boldsymbol{\ell}}|^2 \\ &\leq \sum_{\boldsymbol{\ell} \in \mathbb{I}_{d,N}} w_{\boldsymbol{\ell}} |p_{\boldsymbol{\ell}}|^2 \sum_{\boldsymbol{\ell}' \in \mathbb{I}_{d,N'}} \frac{1}{w_{\boldsymbol{\ell}}} \left| t_{\boldsymbol{\ell}',\boldsymbol{\ell},h} - t_{\boldsymbol{\ell}',\boldsymbol{\ell}} \right|^2 \leq C \left\| u^{\rm inc} \right\|^2_{X_{\boldsymbol{w}}} \left\{ \sum_{\boldsymbol{\ell} \in \mathbb{I}_{d,N}} \frac{[\epsilon(\boldsymbol{\ell})]^2}{w_{\boldsymbol{\ell}}} \right\}. \end{aligned} \tag{3.33}$$

Since

$$\left\| u^\infty - u^\infty_{(N',N,h)} \right\|^2_{L^2(\mathbb{S}^{d-1})} \leq 2 \left\| u^\infty - u^\infty_{(N',N)} \right\|^2_{L^2(\mathbb{S}^{d-1})} + 2 \left\| u^\infty_{(N',N,h)} - u^\infty_{(N',N)} \right\|^2_{L^2(\mathbb{S}^{d-1})},$$

Theorem 3.5 and (3.33) furnish the following result for the fully discrete reduced basis T-matrix method.

Theorem 3.8 *If* $u^{\mathrm{inc}} \in X_w(\partial D)$ *and* $N' > Rk/2$,

$$\left\|u^\infty - u^\infty_{(N',N,h)}\right\|^2_{L^2(\mathbb{S}^{d-1})} \le C \left\|u^{\mathrm{inc}}\right\|^2_{X_{\boldsymbol{w}}} \cdot \left\{ \left(\frac{Rke}{2N'}\right)^{2N'} \sum_{\boldsymbol{\ell}\in\mathbb{I}_d} \frac{1}{w_{\boldsymbol{\ell}}} \left(\frac{\rho_D}{R}\right)^{2|\boldsymbol{\ell}|} |\boldsymbol{\ell}|^{d/2-1} + \sum_{\boldsymbol{\ell}\in\mathbb{I}_d\setminus\mathbb{I}_{d,N}} \frac{1}{w_{\boldsymbol{\ell}}} \left(\frac{\rho_D}{R}\right)^{2|\boldsymbol{\ell}|} |\boldsymbol{\ell}|^{d/2-1} + \sum_{\boldsymbol{\ell}\in\mathbb{I}_{d,N}} \frac{[\epsilon(\boldsymbol{\ell})]^2}{w_{\boldsymbol{\ell}}} \right\}. \tag{3.34}$$

For stable on-line computations, it is important to have a guaranteed accuracy for all off-line computations, that is, $\epsilon(\boldsymbol{\ell}) \le \epsilon$ for all $\boldsymbol{\ell} \in \mathbb{I}_{d,N}$. Henceforth, we assume this. Then, in the case of plane-wave incidence (see Sect. 3.1), by the definition (3.15) of the weights we obtain analogously to (3.19)

$$\sum_{\boldsymbol{\ell}\in\mathbb{I}_{d,N}} \frac{1}{w_{\boldsymbol{\ell}}} \le \sum_{\boldsymbol{\ell}\in\mathbb{I}_d} \left(\frac{Rke}{2|\boldsymbol{\ell}|}\right)^{2|\boldsymbol{\ell}|} |\boldsymbol{\ell}|^d \le \sum_{j=1}^{\infty} \left(\frac{Rke}{2j}\right)^{2j} (2j)^{2d-2} \le C((Rk)^2 + e^{Rk}(Rk)^{2d-1}) \,. \tag{3.35}$$

for $C \approx 10$, see Figure 4. The ultimate bound in (3.35) was found by numerical experiments.

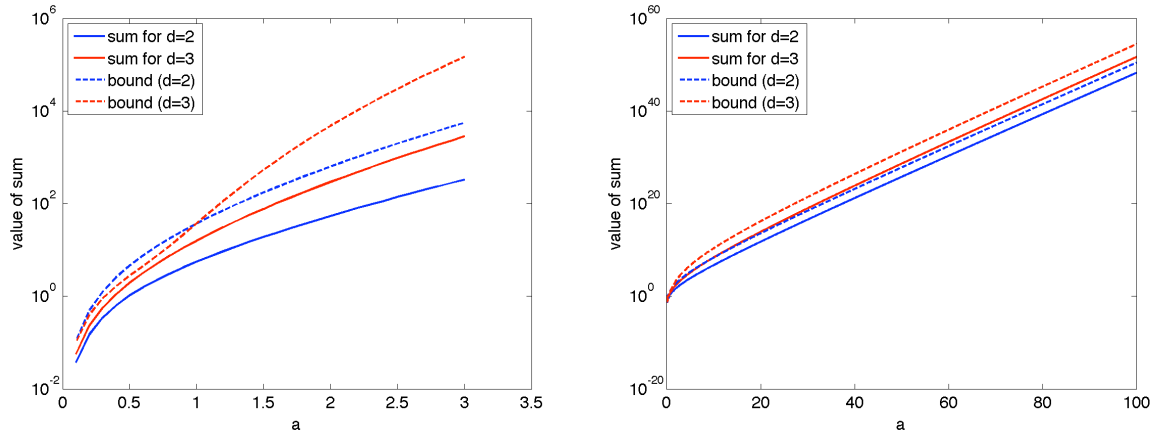

Figure 4: Values of $\sum_{\boldsymbol{\ell}\in\mathbb{I}_d} \left(\frac{ae}{2|\boldsymbol{\ell}|}\right)^{2|\boldsymbol{\ell}|} |\boldsymbol{\ell}|^d$ with $a > 0$ and bounds from (3.35) with $C = 10$.

Hence, from Theorem 3.8 in combination with Theorem 3.6 we get the following convergence result the far-field computed using the fully discrete reduced basis T-matrix $T_{N',N,h}$.

Theorem 3.9 *Let* $u^{\mathrm{inc}}(\boldsymbol{x}) = \exp(ik\boldsymbol{x}\cdot\widehat{\boldsymbol{d}})$, $d = 2, 3$ *and assume* $N' > Rk/2$ *and* $N > RK/2 + d - 1$. *Then*

$$\left\|u^\infty - u^\infty_{(N',N,h)}\right\|^2_{L^2(\mathbb{S}^{d-1})} \le C\Big\{ e^{Rk}(Rke/2)^{3d/2-1} \left(\frac{Rke}{2N'}\right)^{2N'} + N^{3d/2-1} \left(\frac{\rho_D ke}{2N}\right)^{2N} + ((Rk)^2 + e^{Rk}(Rk)^{2d-1})\epsilon^2 \Big\}, \tag{3.36}$$

with $C > 0$ depending only on D and Rk.

In the case of point-source incidence (see Sect. 3.2) one finds, *cf.* (3.27),

$$\sum_{\boldsymbol{\ell}\in\mathbb{I}_{d,N}} \frac{1}{w_{\boldsymbol{\ell}}} \leq \sum_{\boldsymbol{\ell}\in\mathbb{I}_d} |\boldsymbol{\ell}|^d \left(\frac{R}{|\boldsymbol{x}_0|}\right)^{2|\boldsymbol{\ell}|} \leq \frac{C}{(1-(R/|\boldsymbol{x}_0|)^2)^{2d-1}} \,. \tag{3.37}$$

Again using Theorem 3.8, for the point-source induced incident waves, we get the following convergence result for the far-field computed using the fully discrete reduced basis T-matrix $T_{N',N,h}$.

Theorem 3.10 *For $d = 2, 3$, let u^{inc} be as in (3.21) with $|x_0| > R$. For $N' > Rk/2$,*

$$\left\|u^\infty - u^\infty_{(N',N,h)}\right\|^2_{L^2(\mathbb{S}^{d-1})} \leq \frac{C}{(1-(R/|\boldsymbol{x}_0|)^2)^{2d-1}} \left\{ \left(\frac{Rke}{2N'}\right)^{2N'} + N^q \left(\frac{\rho_D}{|\boldsymbol{x}_0|}\right)^{2N} + \epsilon^2 \right\} , \tag{3.38}$$

with $q = 2$ for $d = 2$, $q = 4.5$ for $d = 3$.

4 Numerical Results

In this section we investigate numerically the estimates of Theorem 3.6 and Theorem 3.7 by showing exponential convergence of the simulated far-field for several two dimensional and three dimensional sound-soft scatterers. For each obstacle we simulate scattering of incident plane-waves and of waves originating from point-sources outside a ball of radius ρ_D circumscribing the scatterer.

Our three dimensional obstacles are a sphere and a non-convex obstacle that models an erythrocyte (a red blood cell) [19]. Our two dimensional obstacles are their two dimensional cross section counterparts, namely, a circle and a peanut shaped Cassini-Oval [11]. All of our scatterers are normalized so that they have unit diameter, that is $\rho_D = 0.5$. In our point-source experiments, we chose $|\boldsymbol{x}_0| = 3$ so that $\rho_D/|\boldsymbol{x}_0| = 0.17$.

In all our experiments, for various parameter values $N' = N$, we first compute entries of the reduced basis truncated T-matrix $T_{N,N,h}$ using (3.30), with $S^\infty \widetilde{E}_{\boldsymbol{\ell}}, \boldsymbol{\ell} \in \mathbb{I}_d$ computed with high-accuracy using the high-order algorithm in [7] for $d = 3$ and in [3] for $d = 2$. In order to demonstrate the exponential convergence of our reduced basis T-matrix algorithm, the discretization parameters in these high-order algorithms were chosen, based on various experiments, so that ϵ in (3.29) is of the order 10^{-15} for the circle and sphere and 10^{-10} for the non-convex obstacles. This ensures that for our experiments, the terms with $\epsilon^2 < 10^{-20}$ are much smaller than the other terms in (3.36) and (3.38) and hence we omit the index h.

Using $T_{N,N}$, we computed the approximate far-field $u^\infty_{(N,N)}$ via (3.31), and the scattered-field $u^{\mathrm{s}}_{(N',N)}$ with $E^\infty_{\boldsymbol{\ell}'}$ in (2.46) replaced with $E_{\boldsymbol{\ell}'}$.

For the circle and sphere obstacles, the far-field induced by the incident plane-wave or point-source is known analytically in (Mie) series form. Using the optimal truncation parameter in [8, 18] (which depends on $k\rho_D$), we truncate the Mie series to very high

accuracy and obtain the true far-field u^∞. Thus for these obstacles we are able to compute the relative error

$$e_N = \frac{\left\| u^\infty - u^\infty_{(N,N)} \right\|_{L^2(\mathbb{S}^{d-1})}}{\left\| u^\infty \right\|_{L^2(\mathbb{S}^{d-1})}} \tag{4.1}$$

in our approximation $u^\infty_{(N,N,h)}$ to the true far field u^∞.

The erythrocyte and Cassini-Oval scatterers are considered challenging obstacles for scattering simulations because they have non-convex regions that give rise to multiple reflections. The scattered field for these scatterers is not known analytically. For these scatterers we demonstrate the convergence of the approximation $u^\infty_{(N,N)}$ with respect to N by tabulating

$$e_N = \frac{\left\| u^\infty_{(M,M)} - u^\infty_{(N,N)} \right\|_{L^2(\mathbb{S}^{d-1})}}{\left\| u^\infty_{(M,M)} \right\|_{L^2(\mathbb{S}^{d-1})}} \tag{4.2}$$

where $u^\infty_{(M,M)}$ is a reference solution, computed using the T-matrix with M fixed sufficiently large so that the reference solution is a highly accurate approximation to the exact far field. We approximate the $L_2(\mathbb{S}^{d-1})$-norms in (4.1) and (4.2) using Parseval's inequality. Using (3.13) and (3.22), it is easy to see that e_N in (4.1) and (4.2) is independent of the choice of R used in theoretical analysis for estimating errors in (3.20) and (3.28).

Values of e_N in Figures 5–8 substantiate the exponential convergence established in Theorem 3.6 and 3.7 for the plane-wave and point-source incidence, respectively, on a circle, sphere, peanut, and erythrocyte with $k = 10, 100$. In addition, these figures demonstrate that the theoretical bounds are optimal for some appropriate choice of C and R in (3.20) and (3.28). For each plot in Figures 5–8, the constant C was obtained by fitting with the last data e_N, leading to an appropriate value R closely matching the experimental observation.

One of the advantages of the offline computation and storage of the reduced basis T-matrix is the quick online computation of the acoustic cross section for many different incident fields. In particular, this is very useful to simulate the monostatic ACS, requiring thousands of incident directions. In Figures 9–10 we visualize our reduced basis T-matrix based monostatic ACS simulations for $k = 100$.

In Figures 11–12, for $k = 100$, we visualize the reduced basis T-matrix based total-field outside the ball of radius $R = \rho_D + 0.05$ circumscribing the non-convex obstacles of radius ρ_D for plane-wave (with incident direction $\boldsymbol{x}(\pi/6)$) impinging on the Cassini-Oval and a point-source (located at $-\boldsymbol{x}(5\pi/6, 0)$) induced incident wave impinging on the erythrocyte.

Acknowledgments Part of this work was carried out while M. Ganesh was a Forschunginstitute für Mathematik (FIM) guest at ETH, Zurich. Support of the FIM and the Colorado Golden Energy Computing Organization (GECO) are gratefully acknowledged. Computations were carried out using the GECO cluster Ra.

References

[1] M. Abramowitz and I. Stegun. *Handbook of Mathematical Functions*. Dover Publications, New York, 1970.

[2] S. M. B. Afonso, P. R. M. Lyra, T. M. M. Albuquerque, and R. S. Motta. Structural analysis and optimization in the framework of reduced-basis method. *Struct. Anal. Multidisci. Optimization*, 40:177–199, 2010.

[3] A. H. Barnett and T. Betcke. Stability and convergence of the method of fundamental solutions for Helmholtz problems on analytic domains. *J. Comp. Phys.*, 227:7003–7026, 2008.

[4] D. Colton and R. Kress. *Inverse Acoustic and Electromagnetic Scattering Theory*. Springer, 1998.

[5] A. Doicu, T. Wriedt, and Y. Eremin. *Light Scattering by Systems of Particles. Null-Field Method with Discrete Sources - Theory and Programs*. Springer Verlag, 2006.

[6] W. Freeden, T. Gervens, and M. Schreiner. *Constructive Approximation on the Sphere*. Oxford University Press, 1998.

[7] M. Ganesh and I. G. Graham. A high-order algorithm for obstacle scattering in three dimensions. *J. Comput. Phys.*, 198:211–242, 2004.

[8] M. Ganesh and S. C. Hawkins. Improved high-order algorithms for Mie scattering. *WSEAS Trans. Math.*, 5:663–670, 2006.

[9] M. Ganesh and S. C. Hawkins. A far-field based T-matrix method for three dimensional acoustic scattering. *ANZIAM J.*, 50:C121–C136, 2008.

[10] M. Ganesh and S. C. Hawkins. A far-field based T-matrix method for two dimensional obstacle scattering. *ANZIAM J.*, 51:C201–C216, 2009.

[11] J. Hellmers, E. Eremina, and T. Wriedt. Simulation of light scattering by biconcave Cassini ovals using the nullfield method with discrete sources. *J. Opt. A: Pure Appl. Opt*, pages 1–9, 2006.

[12] A. Kirsch. The denseness of the far field paterns for the transmission problem. *IMA J. Appl. Math.*, 37:213–225, 1986.

[13] P. A. Martin. *Multiple Scattering: Interaction of Time-Harmonic Waves with N Obstacles*. Cambridge University Press, 2006.

[14] M. I. Mishchenko, L. D. Travis, and A. A. Lacis. *Multiple Scattering of Light by Particles: Radiative Transfer and Coherent Backscattering*. Cambridge University Press, 2006.

[15] M. I. Mishchenko, L. D. Travis, and D. W. Mackowski. T-matrix computations of light scattering by nonspherical particles: a review. *J. Quant. Spectrosc. Radiat. Transfer*, 55:535–575, 1996.

[16] A. T. Patera and G. Rozza. *Reduced Basis Methods and A Posteriori Error Estimation for Parametrized Partial Differential Equations*. (c)M.I.T.. MIT Pappalardo Graduate Monographs in Mechanical Engineering,, to appear. (`http://augustine.mit.edu/methodology/methodology_book.htm`).

[17] P. Waterman. Matrix formulation of electromagnetic scattering. *Proc. IEEE*, 53:805–812, 1965.

[18] W. J. Wiscombe. Improved Mie scattering algorithms. *Applied Optics*, 19:1505–1509, 1990.

[19] T. Wriedt, J. Hellmers, E. Eremina, and R. Schuh. Light scattering by single erythrocite: Comparison of different methods. *J. Quant. Spectrosc. Radiat. Transfer*, 100:444–456, 2006.

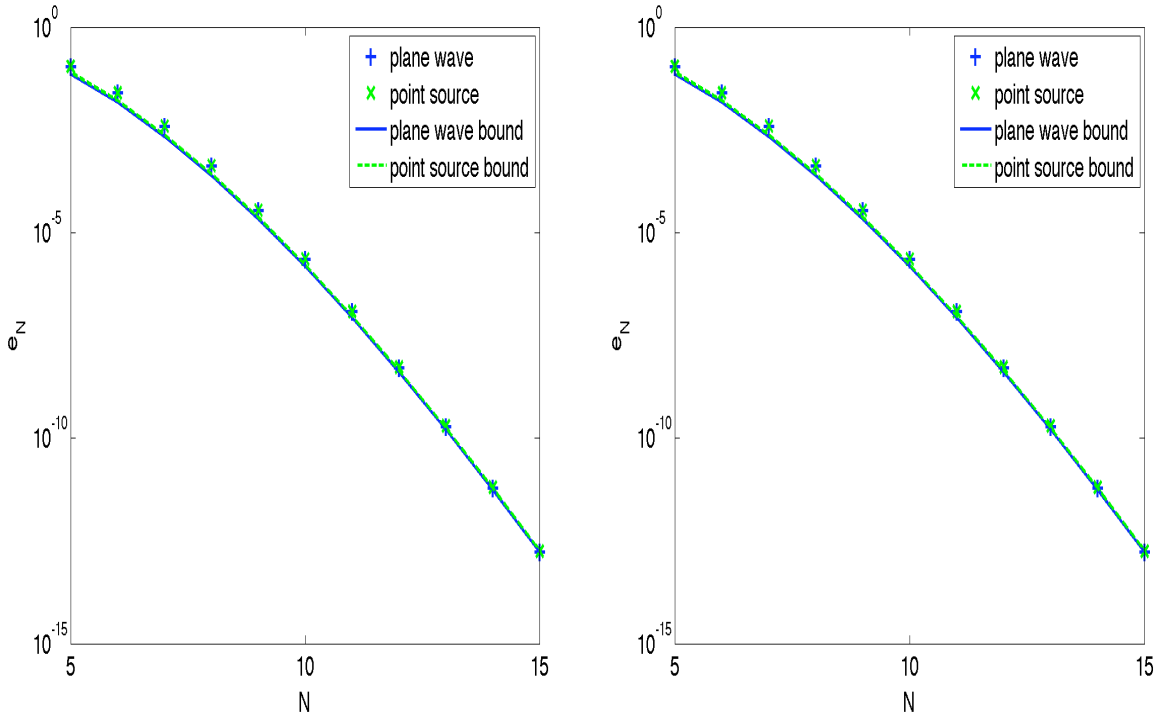

Figure 5: Error e_N in (4.1) and theoretical bounds in (3.20) and (3.28) for plane-wave and point-source incidence (with $\mathbf{k} = \mathbf{10}$) on a circle (left) and a sphere (right).

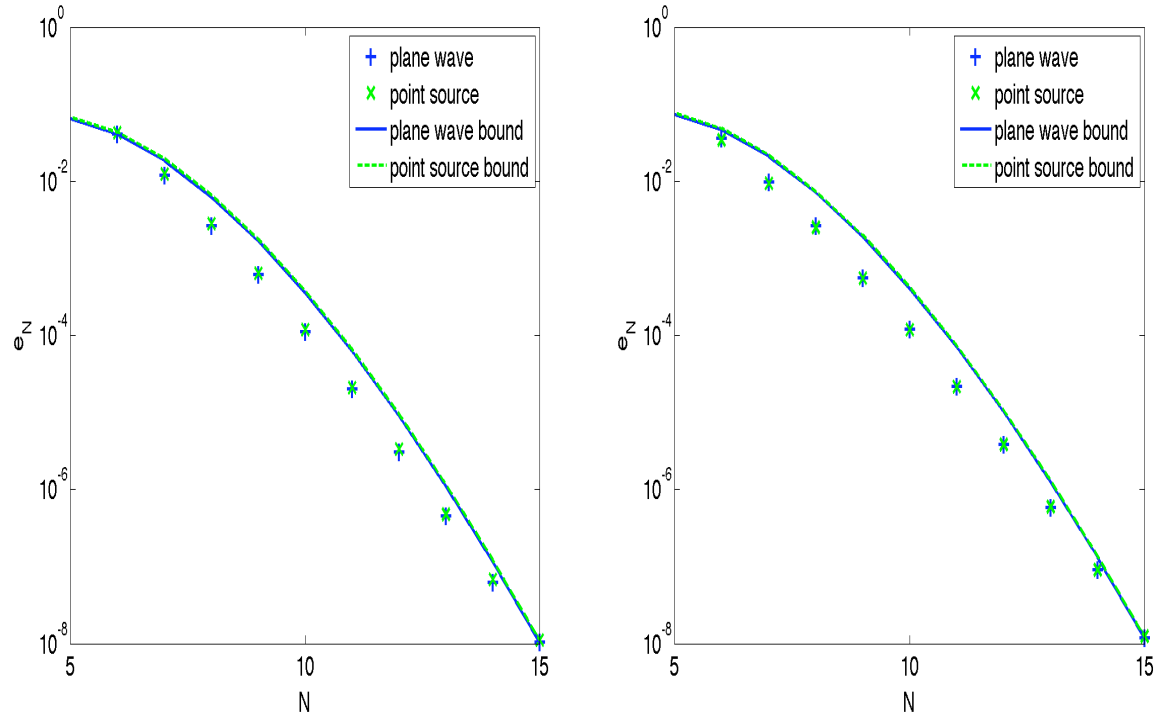

Figure 6: Error e_N in (4.2) and theoretical bounds in (3.20) and (3.28) for plane-wave and point-source incidence (with $\mathbf{k} = \mathbf{10}$) on a peanut (left) and an erythrocyte (right).

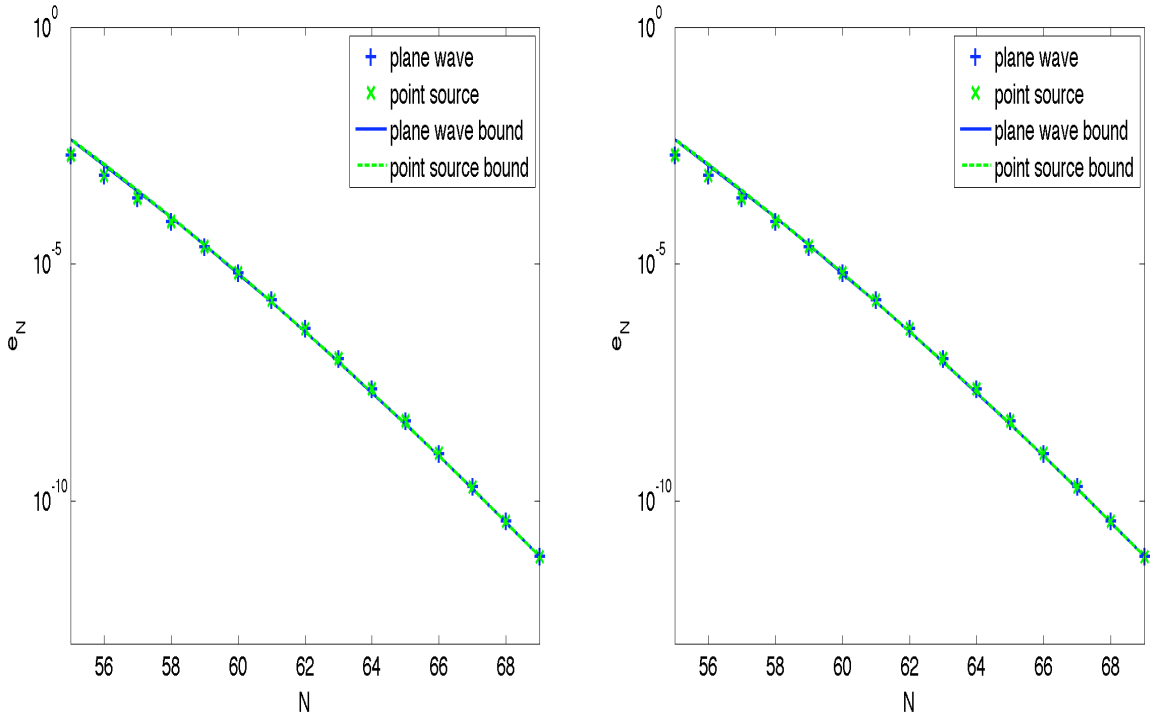

Figure 7: Error e_N in (4.1) and theoretical bounds in (3.20) and (3.28) for plane-wave and point-source incidence (with $\mathbf{k} = \mathbf{100}$) on a circle (left) and a sphere (right).

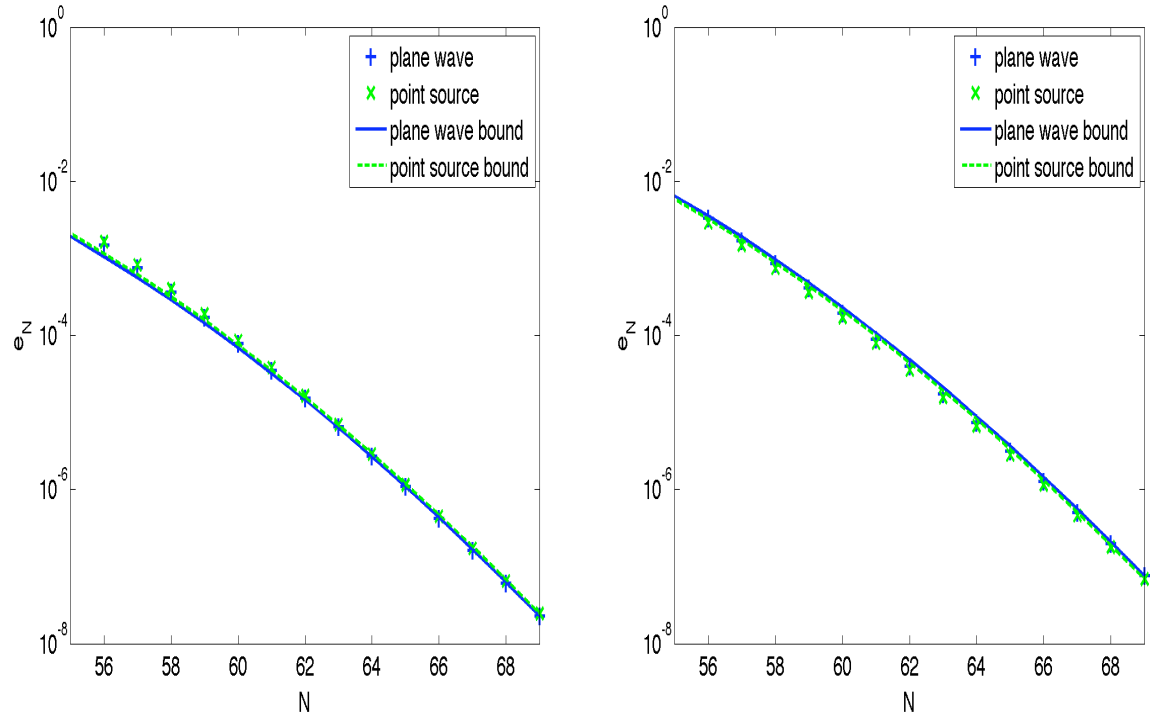

Figure 8: Error e_N in (4.2) and theoretical bounds in (3.20) and (3.28) for plane-wave and point-source incidence (with $\mathbf{k} = \mathbf{100}$) on a peanut (left) and an erythrocyte (right).

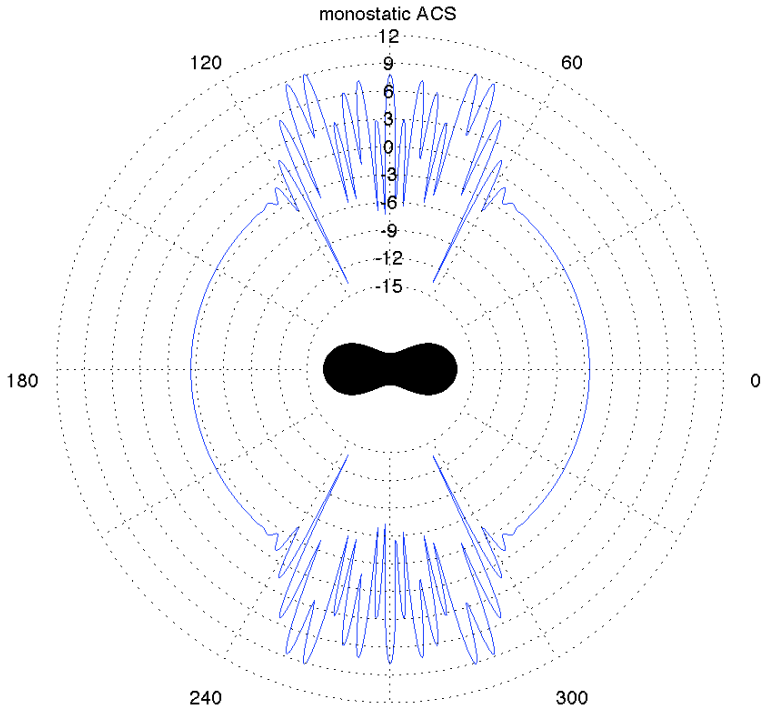

Figure 9: Monostatic ACS of Cassini-Oval (2D) for plane wave incidence with $k = 100$.

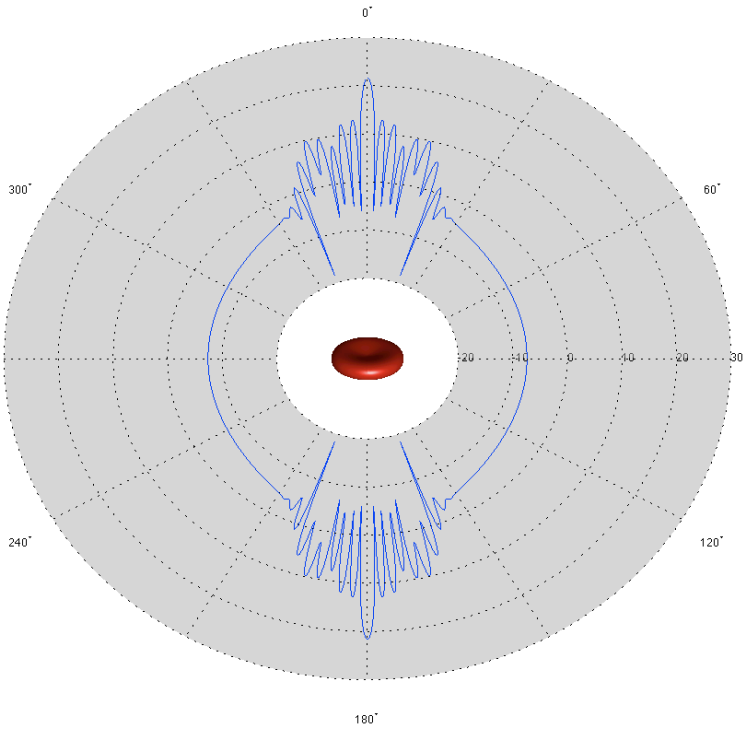

Figure 10: Monostatic ACS of Erythrocyte (3D) for plane wave incidence with $k = 100$.

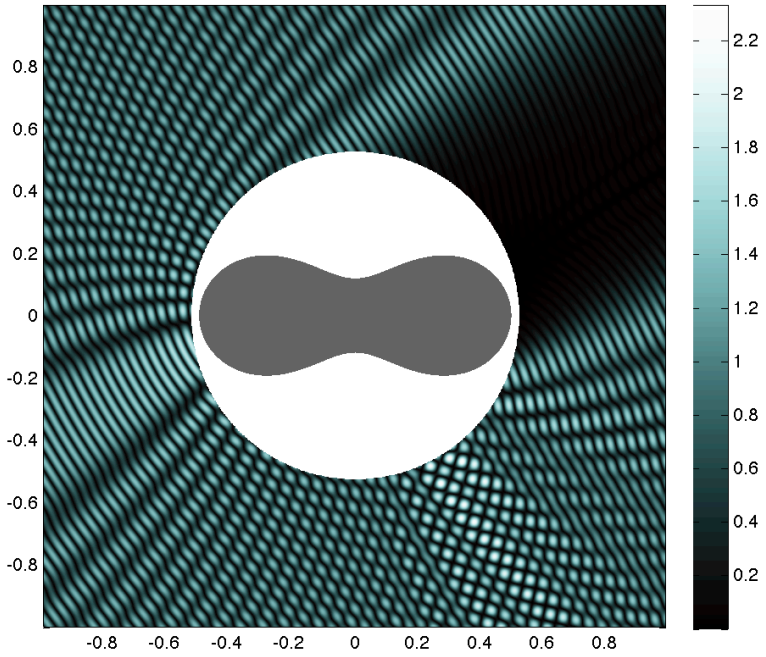

Figure 11: Total exterior field of Cassini-Oval (2D) for plane wave incidence with $k = 100$.

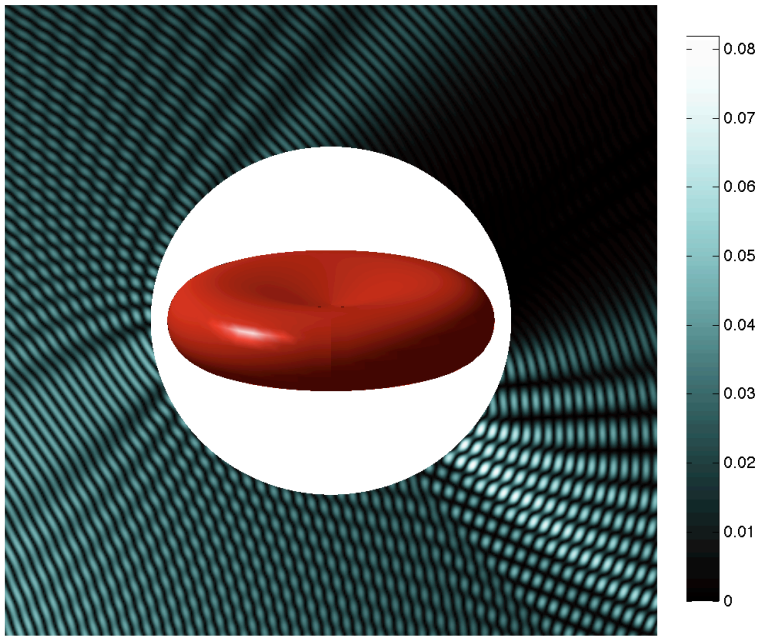

Figure 12: Total exterior field of erythrocyte (3D) for point source incidence with $k = 100$.

Research Reports

No.	Authors/Title
11-04	*M. Ganesh, S.C. Hawkins and R. Hiptmair* Convergence analysis with parameter estimates for a reduced basis acoustic scattering T-matrix method
11-03	*O. Reichmann* Optimal space-time adaptive wavelet methods for degenerate parabolic PDEs
11-02	*S. Mishra, Ch. Schwab and J. Šukys* Multi-level Monte Carlo finite volume methods for nonlinear systems of conservation laws in multi-dimensions
11-01	*V. Wheatley, R. Jeltsch and H. Kumar* Spectral performance of RKDG methods
10-49	*R. Jeltsch and H. Kumar* Three dimensional plasma arc simulation using resistive MHD
10-48	*M. Swärd and S. Mishra* Entropy stable schemes for initial-boundary-value conservation laws
10-47	*F.G. Fuchs, A.D. McMurry, S. Mishra and K. Waagan* Simulating waves in the upper solar atmosphere with Surya: A well-balanced high-order finite volume code
10-46	*P. Grohs* Ridgelet-type frame decompositions for Sobolev spaces related to linear transport
10-45	*P. Grohs* Tree approximation and optimal image coding with shearlets
10-44	*P. Grohs* Tree approximation with anisotropic decompositions
10-43	*J. Li, H. Liu, H. Sun and J. Zou* Reconstructing acoustic obstacles by planar and cylindrical waves
10-42	*E. Kokiopoulou, D. Kressner and Y. Saad* Linear dimension reduction for evolutionary data
10-41	*U.S. Fjordholm* Energy conservative and -stable schemes for the two-layer shallow water equations
10-40	*R. Andreev and Ch. Schwab* Sparse tensor approximation of parametric eigenvalue problems